COURSE 1

TWO-DIMENSIONAL TURBULENCE

JOEL SOMMERIA

PHOTO: height 7.5cm, width 11cm

Contents

1 Introduction **3**

2 Equations and conservation laws **7**
2.1 Euler vs Navier-Stokes equations: 7
2.2 Vorticity representation: 8
2.3 Conservation laws: 9
2.4 Steady solutions of the Euler equations: 12

3 Vortex dynamics **13**
3.1 Systems of discrete vortices: 13
3.2 Vortex pairs 14
3.3 Instability of shear flows and vortex lattices: 18
3.4 Statistical mechanics of point vortices: 20

4 Spectral properties, energy and enstrophy cascade **27**
4.1 Spectrally truncated equilibrium states: 27
4.2 The enstrophy and inverse energy cascades of forced turbulence: . 30
4.3 The enstrophy cascade of freely evolving turbulence: 37
4.4 The emergence and evolution of isolated vortices: 38

5 Equilibrium statistical mechanics and self-organization **40**
5.1 Statistical mechanics of non-singular vorticity fields: 40
5.2 The Gibbs states: 43
5.3 Tests and discussion: 47

6 Eddy diffusivity and sub-grid scale modeling **49**
6.1 Thermodynamic approach: 49
6.2 Kinetic models 53

7 Conclusions: **55**

TWO-DIMENSIONAL TURBULENCE

Joel Sommeria

LEGI/CORIOLIS, 21 avenue des Martyrs, 38000 Grenoble, France.
sommeria@hmg.inpg.fr
http://www.coriolis-legi.org

Contents

1 Introduction

Courses on turbulence generally begin with the delicate question of defining turbulence. As usual for important concepts, a clearcut definition is not possible,

and the problem is still worse for two-dimensional (2D) turbulence. It can be said that turbulence is a flow which is disordered in time and space. The following properties more precisely characterize turbulence, see for instance Lesieur [64]

-Unpredictability of flow realization , in the sense of amplification of small errors (but the statistical properties are generally quite reproducible).

-Continuum flow phenomena, governed by the equations of fluid mechanics (which excludes for instance Brownian motion), and dominated by advective inertial effects (which excludes random wave phenomena, dominated by some restoring force).

-Interaction of a wide range of eddy scales (spatial complexity), which implies high Reynolds numbers and excludes chaos of low-dimensional dynamical systems.

-Increased mixing properties for transported quantities (e.g. chemicals, heat)

Then 2D turbulence is naturally defined as a turbulent flow depending only on two space coordinates x, y or alternatively as a flow confined to a surface (which does not need to be plane, for instance a sphere). In the former case, there is a possibly non-zero third velocity component u_z, along the z direction, but independent of z. Then the equation of motion states

© EDP Sciences, Springer-Verlag 1999

that this velocity component is passively transported (like the concentration of a chemical) by the flow u_x, u_y in the plane, so this third velocity component can be ignored in the theoretical description.

Two additional properties are often considered in defining turbulence (see e.g. Tennekes and Lumley [103]): the existence of strong vorticity fluctuations and strong energy dissipation. Although vorticity dynamics is also essential in 2D turbulence, there is no mechanism of vorticity amplification. We shall see in section 2 that as a consequence energy dissipation is forbidden in the limit of small viscosity: this is the main dynamical signature of a 2D turbulence dynamics. In that sense, 2D turbulence is quite different from usual turbulence, but still the defining properties listed above can be satisfied in two dimensions.

Fig. 1. Grid turbulence in a soap film (from M. Rutgers, 1996 (http://www.physics.ohio-state.edu/~maarten). The fluid is moving from left to right, at velocity 2 m/s, across the comb with mesh 0.3 cm, while the total width is 4 cm. Visualization is provided by interference fringes due to small fluctuations of the film thickness (this is like the color patterns in usual soap bubbles). The increase of turbulent scale with distance to the grid is clearly visible, and it has been measured by laser Doppler velocimetry [71] . Note that this technique for producing 2D turbulence has been first developed by Couder [30]

The very existence of 2D turbulence has been questioned in the past. It has been considered as "a statistical extension of XIX th century fluid dynamics", limited to ideal 2D flow problems remote from the real physical world. Indeed the two cases of 2D turbulence considered above may

seem at first sight equally unrealistic: z independent flows are (by definition) unstable when they become turbulent, and develop three-dimensional instabilities, while confinement to a thin layer requires external forces associated with severe friction effects or other perturbations. At the beginning of a classical review paper on 2D turbulence by Kraichnan and Montgomery [58], 20 years ago, it was said that "Two-dimensional turbulence has the special distinction that it is nowhere realized in nature or in the laboratory but only in computer simulations". Since then, laboratory realization have been obtained for an astounding variety of physical configurations: thin liquid films (Fig. 1), flows in rotating tanks, liquid metal flows or electron plasma in the presence of a uniform magnetic field. Observations of eddy fields in the ocean, or in Jupiter's atmosphere (Fig. 2) provide a strong motivation for studies of 2D turbulence. These systems are more closely approached by 2D turbulence concepts than the Earth atmosphere, for which the thermal forcing and the friction by 3D turbulence in the boundary layer have important influence (see [66] for a recent discussion of the relevance of 2D turbulence to the Earth atmosphere). The existence of coherent eddies like the Great Red Spot is a striking feature of 2D turbulence, as discussed in sections 3.4 and 5. Of course 2D turbulence can be only an approximation of reality, but the theoretical concepts developed for this ideal case appear more and more useful in understanding the strange properties of turbulence in some real flows, and they can provide quantitative predictions.

Another difficulty for observing 2D turbulence, even for an ideally 2D flow dynamics, is that the onset of turbulence is not guaranteed: for instance simple shear flow, like Poiseuille flow, remain stable at any Reynolds number, which is never the case in usual turbulence: all flows become turbulent at sufficiently high Reynolds number, and reach a seemingly universal Kolmogorov regime. Therefore the influence of the forcing mechanism, or initial condition, is more important than in usual, 3D turbulence. It must be further remarked that 2D turbulence tends to eventually organize into steady coherent flows, loosing the unpredictability character. However this organization is itself the result of spatial complexity and mixing occurring in a transient stage.

Beside its practical relevance, a strong incentive to study 2D turbulence is its strange statistical properties, which were recognized in the early theoretical studies, in particular by Onsager (1949) [79] and Kraichnan (1967) [56]. The conservation of vorticity by fluid particles prevents the energy cascade towards small scales (see section 4), resulting in the conservation of energy in the limit of small viscosity, in strong contrast with 3D turbulence. The flow organization into steady coherent structures is also a remarkable feature of 2D turbulence, as already mentioned. A reasonable understanding of 2D turbulence is a prerequisite before studying more complex turbulence problems in atmospheric or oceanic contexts.

Fig. 2. The Great Red Spot (top) and White Oval (bottom) of Jupiter are large vortices remaining remarkably coherent among turbulent eddies, as seen here by the Voyager 1 spacecraft in February 1979. The length of the Great Red Spot is 22 000 km. The mean zonal flow made of alternating jets is probably deeply rooted in the fluid planetary interior, while the observed turbulence is limited to a shallow active layer, dynamically separated from below by a stable density stratification. This observation of a very active turbulence, made visible by cloud motion, was a great surprise due to the weak available forcing. The high velocities can only be explained by assuming that the dynamics is fundamentally 2D, with negligible energy dissipation (although it is of course a layer-wise complex system), as shown by the following arguments. The observed clouds are at a pressure level 3 bars, which must be equal to the column weight for the atmosphere above. Since the gravity is 25 ms^{-2}, the corresponding mass is 1.2 10^4 $\mathrm{kg/m}^2$, so the surface density Σ of the active layer has at least this value (we do not know how deep is the active layer below the observed cloud level). With typical velocities U=50 m/s, the corresponding energy density $E = \Sigma U^2/2$ is at least 15 10^6 $\mathrm{J/m}^2$. The free decay time, equal to the forcing time in a permanent regime, is E/P, where P is the injected power. The heat flux coming from the planetary interior is 5 $\mathrm{W/m}^2$, of the same order as the solar heat flux. The efficiency of conversion to mechanical energy by convective effects is not more than the Carnot efficiency, about 1 % since the typical temperature differences involved are only a few K, for a mean temperature 200 K. Therefore the forcing power is of $P \sim 0.05$ $\mathrm{W/m}^2$, so the decay time E/P is at least 30 10^7s, ten earth years, much longer than the eddy turnover time of a few days. For 3D turbulence, the decay time would be by contrast of the same order as the turnover time.

2 Equations and conservation laws

2.1 Euler vs Navier-Stokes equations:

Turbulence is generally described as a complex solution of the Navier-Stokes equations, restricted here to an incompressible fluid. The status of viscosity in the description of turbulence is a often a subject of debate. The Euler equations (without viscosity) provide the most direct approach, historically also, but lead to many paradoxes, which are avoided by introducing viscosity. Viscous flows are well understood, and going progressively to turbulence by decreasing viscosity is a reassuring approach. The development of bifurcation theories and chaos comforted this view. However the use of viscosity probably skips the true insight into fluid turbulence, whose genuine properties are clearly controlled by inertial effects, which lead to a breakdown of spatial regularity. This is described by the Euler equations. Its strange behavior is repelling, but it may just correspond to the main difficulty of turbulence that cannot be avoided. In 3D turbulence, the introduction of viscosity is justified on physical grounds, as all real fluids are viscous (except superfluid). Furthermore, the regularity of the Euler equations in 3D is not known, so that it may not be a well posed problem (i.e. there is not a unique solution for a given initial condition).

These arguments are not valid in two dimensions. In many physical systems, the motion is not 2D down to the smallest scales. The dissipative mechanisms then depend on the system, for instance they are quite different in atmospheric flows, electron plasma or laboratory scale fluid experiments. Yet properties of 2D turbulence are expected to be common to these different systems. Furthermore, the inviscid equations are well posed: starting from any regular initial velocity field, the Euler equations have a unique regular solution for all time ([108] [54] [2]). This property can be extended to any initial conditions with bounded measurable initial vorticity fields [28], for instance patches with uniform vorticity inside and vorticity discontinuity at the edge.

The inviscid dynamics develops increasing spatial complexity, with smaller and smaller scales of motion. This does not lead to mathematical singularities, as stated above, but actual computations are restricted to a finite resolution, and some smoothing is then necessary. For that purpose we introduce a smoothing operator $\mathcal{V}$, which can be for instance an ordinary Laplacian Δ, a higher order smoothing operator (hyper-viscosity) $(-1)^n\Delta^n$, or some spatial filtering of small scale oscillations. Such smoothing always alters the dynamics to some extent, as it will be discussed in section 6.

Therefore we start with the Euler equations with a smoothing operator $\mathcal{V}$.

$$\partial_t \mathbf{u} + \mathbf{u}.\nabla \mathbf{u} = -\nabla p + \mathcal{V}\mathbf{u} \tag{2.1}$$

$$\nabla.\mathbf{u} = 0 \tag{2.2}$$

$$\mathbf{u}.\mathbf{n} = 0 \ \ , \ \ on\ boundaries(\mathbf{n}\ normal) \tag{2.3}$$

Note that the impermeability boundary condition (2.3) is sufficient for the Euler equations, while a smoothing operator requires an additional condition, whose choice is not obvious. The choice of a physical viscosity, with no-slip condition, may not be appropriate, as physical effects beyond the 2D model often occur in boundary layers, and resolving the thin boundary layer raises numerical difficulties at high Reynolds number. To avoid boundary problems, periodic boundary conditions (equivalent to a toric surface), or a spherical geometry, are often considered for fundamental studies.

2.2 Vorticity representation:

It is often convenient to use a representation in terms of vorticity $\omega(t, \mathbf{r})$ and stream function $\psi(t, \mathbf{r})$,

$$\omega = (\nabla \times \mathbf{u})_z \tag{2.4}$$

$$\mathbf{u} = \nabla \times (\psi \mathbf{e_z}) \equiv -\mathbf{e_z} \times \nabla\psi \tag{2.5}$$

$$\partial_t \omega + \mathbf{u}.\nabla\omega = \nabla \times (\mathcal{V}\mathbf{u}) \tag{2.6}$$

We can identify the vorticity vector, along the z direction (with unit vector $\mathbf{e_z}$), with its z component, a scalar. The evolution equation (2.6), obtained by taking the curl of (2.1) just states that vorticity is advected and conserved by the flow (in the absence of the smoothing operator $\mathcal{V}$). The stream function ψ and resulting flow $\mathbf{u}$ are themselves determined from the vorticity field by solving the Poisson equation, obtained by combining (2.5) and (2.4),

$$-\Delta\psi = \omega \ \ , \ \ \psi = 0\ on\ boundaries, \tag{2.7}$$

so that the whole flow evolution is determined by the scalar vorticity field only.

This Poisson equation (2.7) can be solved in terms of a Green function $G_\psi(\mathbf{r}, \mathbf{r}')$, representing the flow induced at point $\mathbf{r}$ by a singular point vortex (a Dirac vorticity distribution $\delta(\mathbf{r} - \mathbf{r}')$ located at position $\mathbf{r}'$) ,

$$\psi(t, \mathbf{r}) = \int G_\psi(\mathbf{r}, \mathbf{r}')\omega(t, \mathbf{r}')d^2\mathbf{r}' \tag{2.8}$$

$$with \ \ -\Delta G_\psi = \delta(\mathbf{r} - \mathbf{r}') \ \ , \ \ G_\psi = 0\ on\ boundaries, \tag{2.9}$$

The flows induced by all elementary vorticity elements at positions $\mathbf{r}'$ are summed in the integral (2.8).

Far from boundaries, G_ψ has the axisymmetric form,

$$G_\psi(\mathbf{r},\mathbf{r}') = -(2\pi)^{-1}\ln(|\mathbf{r}-\mathbf{r}'|/L) \tag{2.10}$$

where L is the typical domain size, which comes into play as an additive constant, due to the arbitrary choice $\psi = 0$ at the boundary. The corresponding azimuthal velocity, in $1/|\mathbf{r}-\mathbf{r}'|$, is analogous to the magnetic field produced by a line current representing the vortex line. Near boundaries, the effect of virtual mirror vortices outside the fluid domain must be added.

Such a vorticity representation is particularly useful in 2D. It can be used also in 3D, but the evolution of vorticity is more complex due to vortex stretching, possibly leading to complex singularities, and a vector potential must then replace the scalar stream function.

2.3 Conservation laws:

- **Casimirs:**

The incompressibility $\nabla.\mathbf{u} = 0$ ensures that any material area is conserved as its contour is transported by the fluid motion. Furthermore we have seen that the vorticity scalar ω is conserved for each fluid particle (in the absence of smoothing operator $\mathcal{V}$). This is a consequence of the more general Kelvin's theorem stating that $\omega/H = const.$ for a small vortex tube element with length H, which remains constant in the 2D case. Physically this is due to the conservation of angular momentum for a small fluid element, defined with respect to the center of gravity of the element. The conservation of ω for each fluid element implies that the corresponding value $f(\omega)$ is also conserved for any continuous function f, so that, since the surface element $d^2\mathbf{r}$ is also conserved, any functional of the form

$$\mathcal{C}_f = \int f(\omega)d^2\mathbf{r} \tag{2.11}$$

(called a Casimir integral) is conserved. This can be more straightforwardly demonstrated (for a differentiable function f), by multiplying (2.6) by the derivative $f'(\omega)$, which yields $\partial_t f(\omega) + \nabla.(f(\omega)\mathbf{u}) = f'(\omega)(\nabla\times\mathcal{V}\mathbf{u})$ (taking into account that $\nabla.\mathbf{u} = 0$). The domain integral of the second term transforms into a boundary integral which vanishes due to the impermeability condition $\mathbf{u}.\mathbf{n} = 0$, so that the time derivative

$$\dot{\mathcal{C}}_f = \int f'(\omega)(\nabla\times\mathcal{V}\mathbf{u})d^2\mathbf{r} \tag{2.12}$$

indeed vanishes in the absence of the smoothing operator $\mathcal{V}$.

In the case of a power function $f(\omega) \propto \omega^n$, we get for $n = 1$ and 2 respectively the conservation of the circulation Γ and enstrophy Γ_2 ,

$$\Gamma = \int \omega d^2\mathbf{r} \ , \ \Gamma_2 = \frac{1}{2}\int \omega^2 d^2\mathbf{r} \tag{2.13}$$

With a constant viscosity smoothing operator $\mathcal{V}\mathbf{u} = \nu\Delta\mathbf{u}$, the time evolution (2.12) of these quantities can be rewritten by replacing the integral of a divergence by boundary flux,

$$\dot{\Gamma} = \nu \oint \mathbf{n}.\nabla\omega \ , \ \dot{\Gamma}_2 = -\nu \int (\nabla\omega)^2 d^2\mathbf{r} + \nu \oint \mathbf{n}.\omega\nabla\omega \tag{2.14}$$

(an integration by parts has been used to express $\dot{\Gamma}_2$). Note that the circulation is still conserved in the presence of viscosity, except for possible boundary effects. These vanish for "super-slip" boundary conditions $\mathbf{n}.\nabla\omega = 0$ (but not for the more common "free slip" boundary condition $\omega = 0$). The enstrophy Γ_2 decays by viscous effects in the interior, and boundary effects vanish both for free slip ($\omega = 0$) and super-slip $\mathbf{n}.\nabla\omega = 0$ boundary conditions.

The extrema ω_{min} and ω_{max} of the vorticity field remains constant for the Euler equation (in the absence of forcing or friction effects): vorticity is just transported and cannot be amplified by the inertial flow evolution, unlike in three dimensions (these conservation laws can be also obtained from Casimirs with functions f dominated by the extremal values of ω, for instance $f(\omega) = \exp \pm n\omega$ with n very large). Viscosity can only lower the maximum with time and raise the minimum, as by definition $\Delta\omega \geq 0$ at the vorticity minimum, and $\Delta\omega \leq 0$ at the maximum.

- **Energy:**

The kinetic energy $\mathcal{E} = \frac{1}{2}\int \mathbf{u}^2 d^2\mathbf{r}$ is conserved by the Euler equations. This is easily seen by taking the scalar product of (2.1) with $\mathbf{u}$ (with $\mathcal{V} = 0$). Rewriting the advective term with the classical identity $\mathbf{u}.\nabla\mathbf{u} = \omega \times \mathbf{u} + \nabla(\mathbf{u}^2/2)$, the first term is orthogonal to $\mathbf{u}$, while the second is incorporated in the pressure, and the $\mathbf{u}.\nabla p' = \nabla.(p'\mathbf{u})$, whose domain integral vanishes due to the impermeability condition. Note that this demonstration equally applies in 3D, but it requires differentiability of the velocity field, while we expect that in 3D, energy dissipation would occur after a finite time due to the formation of singularities (then the Euler equations themselves could be only defined in the sense of distributions, not ordinary fields). By contrast, in 2D, the flow remains regular for all times, so energy is truly conserved.

A more classical point of view is to consider the effect of a small viscosity. Then the energy varies as $\dot{\mathcal{E}} = \nu \int \mathbf{u}.\Delta\mathbf{u} d^2\mathbf{r}$. Noting the identities $\Delta\mathbf{u} = -\nabla \times \omega$ (since $\nabla.\mathbf{u} = 0$), and $\mathbf{u}.(\nabla \times \omega) = \nabla.(\omega \times \mathbf{u}) + \omega^2$, we get

$$\dot{\mathcal{E}} = -2\nu\Gamma_2 - \nu \oint (\omega \times \mathbf{u}).\mathbf{n} \tag{2.15}$$

The boundary term vanishes both for the no-slip ($\mathbf{u} = 0$) and free slip ($\omega = 0$) boundary conditions, and the interior term always makes the energy decay, as expected.

The enstrophy Γ_2 also decays by (2.14), in the absence of boundary effects. Then the rate of energy decay (2.15) is bounded by the initial enstrophy, and tends to 0 in the limit of small viscosity ν: energy is conserved in this limit.[1] By contrast in fully developed 3D turbulence the enstrophy increases as the viscosity is reduced (smaller and smaller scales are excited), such that the product of these two quantities, determining the energy dissipation, becomes independent of viscosity: it is controlled by the inertial cascade process.

Hyper-viscosity terms are often introduced in simulations of 2D turbulence to better approach the inviscid limit of zero energy dissipation. Then vorticity fluctuations are smoothed out like with viscosity, the enstrophy Γ_2 decays , but as a spurious effect the extrema ω_{min} and ω_{max} may be amplified (also higher order boundary conditions need to be introduced).

In 2D flows it is often convenient to rewrite the energy using an integration by parts, so that

$$\mathcal{E} = \frac{1}{2} \int \psi\omega d^2\mathbf{r} \tag{2.16}$$

Note that the integration by parts also yields a boundary term $\oint \psi\mathbf{u}.d\mathbf{l}$, but it vanishes thanks to the boundary condition $\psi = 0$. Another choice $\psi = const.$ would introduce a boundary term in $\Gamma \times const.$ which is unimportant as it is constant in time. Note that when considering vortices interacting in a limited region of an infinite domain, the physical energy $\frac{1}{2}\int \mathbf{u}^2 d^2\mathbf{r}$ diverges for a non-zero circulation Γ (as the induced velocity only decays in Γ/r the energy integral logarithmically diverges), and only the form (2.16) can be used (see [4]). This kinetic energy has remarkably the same form as the electrostatic energy of a charge density field ω inducing a potential ψ, satisfying the Poisson equation (2.7).

- **Momentum and angular momentum:**

In an infinite domain the momentum vector $\mathbf{P} = \int \omega\mathbf{r} \times \mathbf{e}_z \; d^2\mathbf{r}$ is conserved, as well as the angular momentum with respect to any origin $L = \int \omega\mathbf{r}^2 \; d^2\mathbf{r}$,

[1] This conclusion is unchanged with other boundary conditions, for instance no-slip: then a boundary layer of thickness $\delta = (\nu L/U)^{1/2}$ forms (U typical velocity), contributing to enstrophy as $\Gamma_2 \sim U^2 L/\delta$. Then the energy dissipation $\nu\Gamma_2$ is in $\nu^{1/2}$, which also tends to zero in the inviscid limit.

see for instance [4] or [23]. These conservation laws are associated with symmetries of the system: invariance by translation for $\mathbf{P}$ and invariance by rotation for L. and they are conserved as well in domains whose boundaries respect these symmetries: the x-wise momentum component is also conserved in a channel along the x-direction (see e.g. [98]), and the angular momentum in a disk (taking the origin at the center). Note that this global angular momentum L has to be distinguished from the local angular momentum of a fluid particle, which is conserved for all geometries.

Finally the circulation $\oint \mathbf{u}.d\mathbf{l}$ along any boundary contour is conserved. For a simply connected domain, this is just the circulation Γ already considered, but the circulation along any obstacle is also conserved, and is not related to $\int \omega d^2\mathbf{r}$, for instance along the inner wall of an annular domain. This conservation law is directly demonstrated from (2.1), rewriting the advective term with the identity $\mathbf{u}.\nabla\mathbf{u} = \omega \times \mathbf{u} + \nabla(\mathbf{u}^2/2)$, whose integral vanishes on the wall since $\omega \times \mathbf{u}$ is normal to the wall (as $\mathbf{u}$ is along the wall due to the impermeability condition) and a closed contour integral of a gradient vanishes.

- **Other conservation laws:**

We have listed here all the explicit conservation laws for the 2D Euler equations: it can be shown [92] that there are no other conserved quantities with an explicit form $\int F(\mathbf{r}, \mathbf{u}(\mathbf{r}), \partial_i u_j(\mathbf{r}))\ d^2\mathbf{r}$. Other conservation laws however exist, for instance "topological constraints": two initial uniform vorticity patches remain always distinct and they cannot fully merge in a single patch. However this constraint plays little role in practice, as the two patches can irreversibly deform and become more and more intertwined in the merging process discussed in next section.

2.4 Steady solutions of the Euler equations:

It is often useful to discuss steady solutions of the 2D Euler equations, as they will appear as the result of turbulent mixing. For steady flows the particle trajectories are streamlines, so that ω, which is conserved along trajectories, will be constant along any streamline. This means that ω is a function of ψ only, at least in some sub-region: $\omega = F(\psi)$. In fact the same value of ψ can occur on several streamlines, so that different functions F can characterize different regions, as will be shown in the example of the dipole, next section. Reciprocally, it is clear that if $\omega = F(\psi)$, then the advective term $\mathbf{u}.\nabla\omega = -\nabla\psi \times \nabla\omega$ vanishes as $\nabla\omega = F'(\psi)\nabla\psi$ is parallel to $\nabla\psi$. Therefore the property of steady flow is indeed equivalent to the property $\omega = F(\psi)$ in subregions. The interface between these subregions must be a streamline with velocity continuous across it (but discontinuous vorticity in general).

It is also useful to consider steadily translating solutions, with a constant translation velocity vector $\mathbf{U}$, such that $\omega(t, \mathbf{r}) = \omega(\mathbf{r} - \mathbf{U}t)$. This is equivalent to a steady solution in a reference frame translating at velocity $\mathbf{U}$, with the same vorticity and stream function $\psi' = \psi - \mathbf{U}.\mathbf{r}$, so that $\omega = F(\psi - \mathbf{U}.\mathbf{r})$. Note that this is only possible in an infinite domain or a channel along the $\mathbf{U}$ direction.

Similarly we can consider purely rotating solutions $\omega(t, \mathbf{r}) = \omega(\mathbf{r} - (\Omega \times \mathbf{r})t)$, which is possible in an infinite domain or a circular geometry (disk or annulus). The general form of such flow patterns in solid body rotation is $\omega = F(\psi + \Omega \mathbf{r}^2/2)$. This can be shown directly on the Euler equations, or by using a rotating reference frame at angular velocity Ω.[2]

3 Vortex dynamics

As turbulence is part of fluid dynamics, it is always useful to keep in mind elementary flow processes. This is particularly true for 2D turbulence, which displays "coherent structures" more clearly than 3D turbulence. Some discussion of inviscid vortex dynamics is therefore useful. Interesting results were already obtained in the XIXth century, and some of them "rediscovered" and extended recently in the context of 2D turbulence and ocean-atmosphere dynamics. The classical textbooks of Lamb (1932) [60] and Batchelor [4] provide good introductions to this field, and more advanced properties of discrete vortices are treated by Chorin [26] [27] and Aref [1], and vortex patches by Saffman [91]. The use of point vortices as a numerical discretization of continuous fluid motion is treated in a recent book by Cottet and Koumoutsakos [29]. The main motivation of the XIXth century researchers was different: they were seeking mechanical models to build theories of electromagnetism and atomic physics.

3.1 Systems of discrete vortices:

Replacing the continuous vorticity field by a set of singular point vortices (or vortex lines in the z direction) can be a good approach to many 2D flow phenomena. Relation (2.8) then reduces to the discrete sum of the flows

[2] While the invariance of the system by translation (Galilean change of reference frame) is warranted as a general physical principle, this is not so for a rotating reference frame, in which centrifugal and Coriolis force appear. However both forces are pure gradients in incompressible 2D flows, so they are exactly balanced by pressure gradients. Indeed the centrifugal force is proportional to $\nabla(\Omega \mathbf{r}^2/2)$, with a constant density factor, and the Coriolis force is proportional to $-2\Omega \times \mathbf{u} = \Omega \nabla \psi$. Note that the so-called geostrophic balance between Coriolis force and pressure gradient is only realized in 2D flows.

induced by each point vortex at position $\mathbf{r}_j(t)$ and circulation γ_j,

$$\psi(t, \mathbf{r}) = \sum_j \gamma_j G_\psi(\mathbf{r}, \mathbf{r}_j(t)). \tag{3.1}$$

Each vortex is transported by the flow induced by all the other vortices. The self interaction of the vortex (leading to a diverging ψ) can be ignored, as seen by defining a point vortex as the limit of small vorticity patches with vorticity $a_i \to \infty$ and infinitely small area γ_i/a_i, such that the circulation γ_i remains constant. Then self-interaction just produces a local rotation of the patch with no influence on the limiting point vortex. Furthermore the circulation γ_i of each vortex is conserved in the flow evolution, since both the small vortex patch area and vorticity a_i are conserved. Thus each vortex i is transported by the velocity derived from the stream function (3.1), with the sum restricted to $i \neq j$ which yields (the sum is made on indices $i < j$ to avoid double counting of the same term),

$$\dot{x}_i = \partial E_{int}/\partial y_i \ \ , \ \ \dot{y}_i = -\partial E_{int}/\partial x_i \tag{3.2}$$

$$with \ \ E_{int} = \sum_{i<j} \gamma_i \gamma_j G_\psi(\mathbf{r_i}, \mathbf{r_j}) \tag{3.3}$$

The N point vortices therefore move like N interacting particles. The study of point vortices was initiated by Helmholtz in 1858, and this general dynamical equation first derived by Kirchhoff.

The dynamical equation is first order in time, unlike the usual second order Newton equation. However it has quite remarkably a Hamiltonian structure, but the conjugate variables are the space coordinates x_i and y_i instead of the positions and momenta of the particles. The Hamiltonian E_{int} is conserved with flow evolution, and it corresponds to an interaction energy of vortices. Note that the true physical energy is infinite due to the self-energy associated with each vortex (the velocity tends to infinity in $1/r$ around each vortex core but this has no influence in the vortex interaction). The expression (2.10) of the interaction energy is like the electrostatic interaction energy for long charged rods (notice however that it corresponds physically to a kinetic energy of the flow, and the analogy with electrostatics is not complete, due to the different dynamical equation). The pair interaction decays only slowly with distance, so that vortex interactions are highly non-local, and we expect collective effects to be important, rather than binary collisions.

3.2 Vortex pairs

- **Case of point vortices:**

Suppose two point vortices of like sign and circulation γ are separated by a distance d far from boundaries. Then (3.2) just states that the two vortices rotate at velocity $\gamma/(2\pi d)$, keeping a constant distance d (Fig. 3a). Two vortices with unequal strength rotate around their "center of mass". If the two vortices have equal circulation with opposite sign, the center of mass does not exist, and both vortices translate with constant spacing d. (Fig.3b)

Note that in superfluids, vortices of opposite sign tend to eventually attract and annihilate each other. This is due to interactions with additional degrees of freedom, which can extracts energy from the fluid system. An external force on a vortex, for instance due to pinning on a solid substrate, can result in drift of the vortex core with respect to the local flow, and the occurrence of a Magnus force perpendicular to this drift, resulting in reduction of the vortex distance. Such effects are absent in the ideal flow problems considered here, and the distance d does remain constant.

In the translating case it is interesting to note that a region of the flow is transported and follows the translating motion. Therefore this flow contains momentum, representing the translating motion of some fluid area, see Fig. 4 left (this is the 2D analog of a vortex ring).

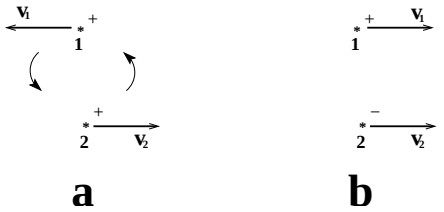

Fig. 3. Sketch of the motion of a vortex pair. (a) rotation with like signs and (b) translation with opposite signs.

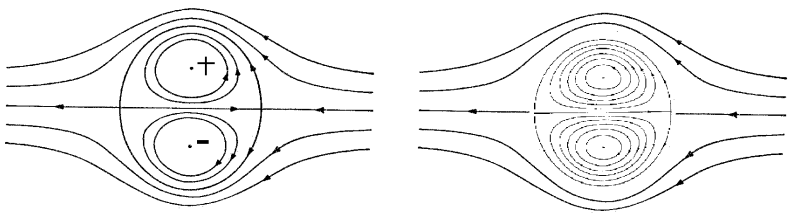

Fig. 4. Flow (left) in a point vortex pair and (right) in a Chaplygin's continuous pair. The streamlines are represented in a reference frame moving with the structure (so the flow is steady). Note that the fluid area inside the closed streamlines is entrained by the pair in its motion.

- **Translating vortex pairs with continuous vorticity:**

The translating motion of vortex pairs with opposite sign is a remarkably robust feature, obtained when flow momentum is injected, even when vortices are far from pointwise. Fig. 5 shows how an initial jet organizes into a vortex pair in a stratified fluid [46]. Similar results had been previously obtained from a wake in a soap film [31] or in an electromagnetically driven flow [77]. We see that, remarkably, the turbulence "self-organizes" into simple coherent structures, here vortex pairs, and this will be the subject of section 5.

A vortex pair solution proposed by Chaplygin in 1902 [15] (see also the review paper [72]) provides a more realistic description of such features, using continuous vorticity fields. We have seen in subsection 2.4 that a general steadily translating solution is obtained with a vorticity of the form $\omega = -\Delta\psi = F(\psi - \mathbf{U}.\mathbf{r})$ in some region. A natural idea is to choose a linear function F, then solving a Helmholtz equation for ψ in the vortex domain, matching an irrotational flow outside with continuous velocity. It turns out that a good matching is then obtained only with a circular domain, and one obtains Chaplygin's solution

$$\psi = -\frac{2U}{k}\frac{J_1(kr)}{J_0(ka)}\sin\theta \;\; for\; r \leq a \;\; , \;\; \psi = U(r - \frac{a^2}{r})\sin\theta \;\; for\; r \geq a \quad (3.4)$$

in terms of the polar coordinates r and θ, where J_0 and J_1 are Bessel functions and ka the first zero of J_1.

Note that this solution, represented in Fig. 4 right, emerges in many experiments and numerical simulations by spontaneous organization after complex flow evolution. Similar asymmetric dipoles, with a rotating motion are also obtained. For any initial momentum, angular momentum, and energy, one can determine a corresponding dipole or axisymmetric monopole solution [23], which is expected to be obtained after complex vorticity stirring in some region of space. However non-linear relationships between vorticity and streamfunction can be obtained as well [77].

- **Vortex merging:**

Two vorticity patches with the same sign rotate around each other like point vortices when their distance is sufficiently large in comparison with their size. Each patch is just slightly deformed by vortex interactions: this is like tidal effects between two gravitating bodies. This is however no longer true below some critical distance: the two vortices irreversibly deform leading to a single vortex, as shown in Fig. 6. This figure is obtained from an experiment with an electron plasma trapped in a magnetic field, which remarkably follows the 2D Euler equations. The flow eventually tends to

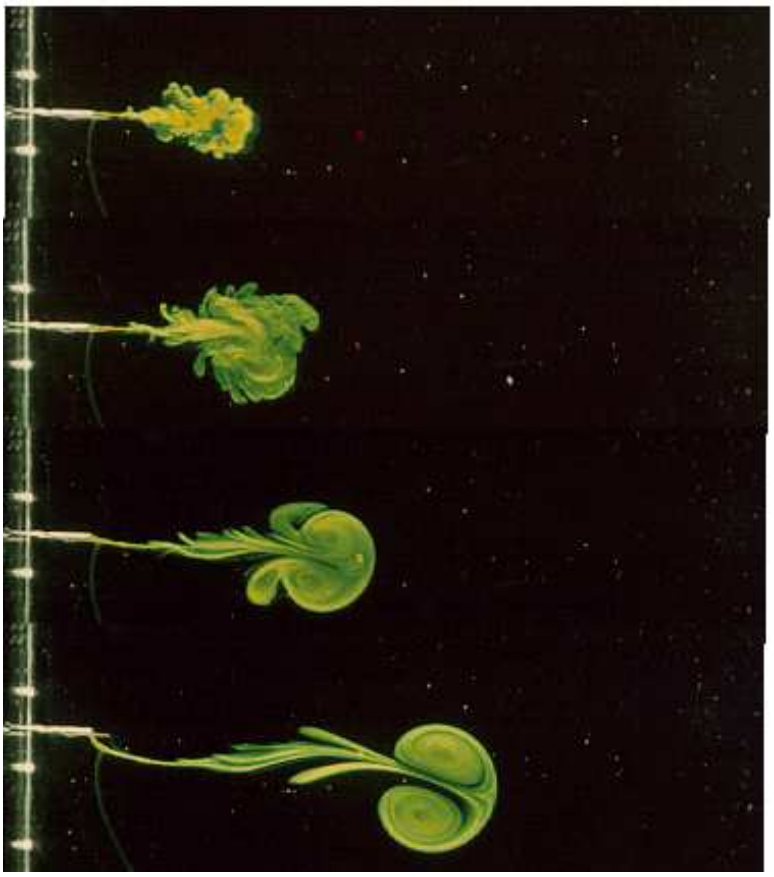

Fig. 5. organization of a short jet injected in a density stratified flow (from ref. [46]). We see in the successive views of the same jet the initial 3D stage, followed by a collapse to a quasi-2D state, which organizes into a dipole.

an axisymmetric configuration when small scale vorticity oscillations are smoothed out. The threshold of distance leading to irreversible deformation has been studied in detail using contour dynamics for vortex patches [81]. The resulting final merging can be understood on general grounds as a process of entropy maximization (see section 5): the most probable state of the system is axisymmetric.

The initial vortex deformation leading to merging is due to the effect of the strain induced by the other vortex. This is a motivation for studying the influence of a uniform pure strain on a single vortex. A weak vortex is clearly passively deformed by the strain, while it resists deformation when

its vorticity reaches a value of the same order as the strain rate.

The same merging mechanism is observed for vortices of unequal size and strength (but equal sign). This has been checked with electron plasma experiments [75] as well as various numerical simulations.[3]

- **Interaction of more than two point vortices:**

Interaction of three point vortices yields a variety of motion. The problem has some similarity [78] with a triad in Fourier space, which shall be discussed in section 4. An interesting curiosity is the possibility, for particular initial conditions and vortex circulations, that the three vortices spiral inward to a singular point [1]. Singularities are however forbidden in the case of more realistic finite core vortices. For four vortices and more, chaotic motion is possible, as well as stable configurations. Tripoles made of a central vortex and two satellite vortices of opposite sign have been observed both in laboratory [48] and oceanic flows. With point vortices, stable patterns are obtained for more than three vortices, but none of them seem robust for extended vortices: two vortices of the same sign tend to merge.

3.3 Instability of shear flows and vortex lattices:

- **Parallel flows:**

The classical stability criterion of Rayleigh applies to 2D inviscid flows. Thus classical flows with vorticity extrema, shear layers, jets and wakes develop 2D turbulence. The turbulent region grows linearly with time or stream-wise coordinate, in a similar way whether or not 3D perturbations are allowed to develop [65].

By contrast Poiseuille flows and boundary layers behave quite differently. These flows are linearly stable according to the Rayleigh criterion (they have no vorticity extrema), and they indeed remain stable in purely 2D flows, whatever the Reynolds number. The instabilities occurring in these flows are genuinely three-dimensional and are suppressed by the constraint of two-dimensionality.

- **Vortex lattices:**

Vortex lattices can initiate 2D turbulence when they are unstable. The square lattice of alternating sign vortices is highly unstable and initiates

[3] Note however that contour dynamics simulations indicate a variety of other possibilities for unequal size vortices [34]: in some cases merging is only partial, and small satellite vortices are produced. Such processes could be relevant in controlling the population of vortices of different size in 2D turbulence as discussed in section 4, so this problem would require more careful examination, comparing different numerical methods.

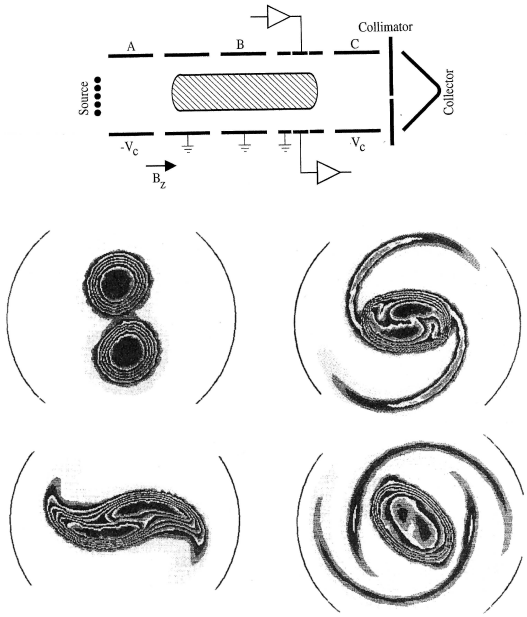

Fig. 6. Vortex merger in an electron plasma experiment (from [75]). Maps of the vorticity field are represented at four successive times (0, 16, 41 and 76 μs). The initial distance of the vortex centers is 1.2 times the vortex diameter. The experimental device is sketched at the top of the figure. The electrons are extracted from a source in the high vacuum cylindrical cell. Then they are transversally confined by the uniform axial magnetic field $\mathbf{B}_z$ and they drift with the velocity $\mathbf{u} = c(\mathbf{E} \times \mathbf{B}_z)/B_z$ perpendicular to the electric field $\mathbf{E}$ induced by the electron space charge. This drift flow remarkably satisfies the Euler equations: the incompressibility condition $\nabla.\mathbf{u} = 0$ is a consequence of $\nabla \times \mathbf{E} = 0$ while the vorticity $\nabla \times \mathbf{u} \propto \nabla.\mathbf{E} = n/\epsilon_0$ is proportional to the charge density n, conserved by the flow. This charge density field is visualized and measured by suddenly accelerating the electrons on the collector (destroying the system).

the inverse energy cascade of 2D turbulence. In contrast, triangular lattices of equal sign vortices and hexagonal lattices with alternating sign vortices turn out to be stable [104]. Such stability properties can be more easily determined if one restricts the analysis to perturbations at large scales with respect to the lattice mesh, so that asymptotic expansions can be used. It is then shown that a minimal degree of anisotropy is needed to get instability [43].

In conclusion, while 3D flows at very high Reynolds systematically develop turbulence, with quasi-universal behavior, this is not true in 2D. There

is much more influence of the generating mechanism, and turbulence may not be produced at all in some cases.

3.4 Statistical mechanics of point vortices:

- **The statistical mechanics approach:**

Statistical mechanics, as developed by Maxwell, Boltzmann, Gibbs and their followers, has been remarkably successful in predicting the behavior of systems with many degrees of freedom. Its main success has been in predicting the statistical (thermodynamic) equilibrium for a conservative (Hamiltonian) systems, for instance a gas made of many molecules. 3D turbulence is, in contrast, a strongly dissipative system. However, 2D turbulence conserves energy, which raises hope for equilibrium statistical mechanics approaches. This is not an obvious matter however, since 2D turbulence undergoes irreversible transformations with dissipation of vorticity fluctuations (enstrophy), instead of energy. The point vortex model is precisely a Hamiltonian system, as we have seen in subsection 3.1, so that the standard methods of equilibrium statistical mechanics readily apply. The relevance to actual continuous flows will be discussed later.

The statistical mechanics of point vortices was first discussed by Onsager in 1949 [79]. First of all, it is an interesting exercise in statistical mechanics, since "negative temperature" states are obtained. In such states vortices of like sign tend to clump together, forming large coherent vortices. Onsager stressed the importance of such coherent structures with remarkable foresight, and he pointed out the fundamental difference with the energy cascade of 3D turbulence, which had been recently formalized by Kolmogorov in 1941. Although short, his paper contains far-reaching remarks on both 2D and 3D turbulence, and its reading is highly recommended.

The general principles of equilibrium statistical mechanics are explained in many textbooks of physics, but this is always a subtle subject. Since applications to 2D turbulence are unusual, they require a good understanding (and re-discussion) of the basic principles, and it may be useful to recall them in the context of vortex dynamics.

The starting point of equilibrium statistical mechanics is to list the *conserved quantities* of the system, which are clear constraints to the dynamics. For a set of many point vortices, the only known conserved quantity is energy, as is the case for usual thermodynamic systems (but we shall see additional conserved quantities with alternative models of 2D turbulence). Then it is assumed that the system evenly explores all its possible states (the "*microscopic states*") allowed by the given value of its conserved quantities (here just energy). This assumption (the *ergodic hypothesis*) has been rigorously demonstrated only for a system of hard spheres in elastic collisions, but is believed to be true in many cases.

The output of the theory is the probability distribution of "*macroscopic*" states of interest, for instance the vortex density field. The *entropy* S of the macroscopic state is defined as the logarithm of the "number" of possible microscopic states corresponding to this macroscopic state. Then it follows from the ergodic hypothesis that the probability of this macroscopic state is just proportional to the exponential of the entropy. The most probable macroscopic state is therefore that which maximizes the entropy. In the limit of a very large number of particles, this maximum tends to be very sharp: an overwhelming majority of microscopic states tends to concentrate near the macroscopic state of maximum entropy. Therefore *deterministic* predictions result from the statistics of many particles, for instance the density of vortices will fluctuate less and less as the vortex density increases.

A microscopic state is defined by the coordinates of each of the N vortices. To count the possible states, we need first to discretize the coordinates into elementary cells. Let us take a mesh h in each coordinate[4](and consider a fluid domain with surface unity for simplicity), so that the total number of possible states for a single vortex is just the cell number $1/h^2$. For N vortices it is $1/h^{2N}$ (we assume that several vortices can occupy the same cell without restriction, which is true for ideal point vortices). Among these states we must select and count the ones which have a given energy E_{int}, rel.(3.3).

This is a tremendous task in general, but let us first neglect this interaction. Then we expect a uniform vortex density. To show this, consider the density field $n(\mathbf{r})$ as the macroscopic state, and let us count the corresponding number of configurations. We make a partition of the fluid domain in p sub-domains, with area $A = 1/p$ each, and consider the vortex numbers $n_1, ...n_p$ in each sub-domain as the macroscopic state. We must first distribute the vortices in packets with $n_1, ...n_p$ vortices respectively. The number of possibilities is $\frac{N!}{n_1!.....n_p!}$ (this is the total number of permutations divided by the number of permutations within each packet, which does not change the distribution). Then for sub-domain 1 the number of possible

[4]The uniform discretization used for the counting seems here a natural choice, but it may be wrong with other coordinates. For instance a uniform discretization in the polar coordinates r, θ would give very small cells $drd\theta$ near the pole, resulting in excessive statistical weight. The justification lies in the Hamiltonian form (3.2) of the dynamical equations, from which the *Liouville theorem* is readily demonstrated: considering the evolution of many identical systems, this theorem states that the volume element $dx_1....dx_N dy_1....dy_N$ in phase space is conserved with time. Indeed the divergence of the "velocity vector" $\dot{x}_1, ..., \dot{x}_N, \dot{y}_1, ...\dot{y}_N$ is clearly 0, due to the Hamiltonian form (it is the analog for the phase space flow of a stream function for a usual 2D flow). Then the uniform sampling in the coordinates $x_1, ..., x_N, y_1....., y_N$ will *remain uniform* with the time evolution of the system. This is only true for the so-called canonical coordinates for which this usual canonical form (3.3) of the Hamiltonian system can be written. It is not the case, for instance, with polar coordinates.

vortex configurations (positions) is $(ph^2)^{-n_1}$ and we have to multiply by the similar formula with the other sub-domains. The number of configurations with $n_1, ...n_p$ vortices is therefore $\frac{N!}{n_1!.....n_p!}(ph^2)^{-N}$. The entropy is the logarithm of this quantity. For large vortex numbers, we can use the Sterling formula, $n! \simeq n \ln n$, so that the entropy is

$$S = -\sum n_i \ln n_i \to -\int n \ln n d^2\mathbf{r} \tag{3.5}$$

in the continuous limit (up to an unimportant constant, depending on the discretization mesh).

Maximizing this entropy with the constraint of a given total vortex number $N = \int n d^2\mathbf{r}$ gives a uniform density. To check that, we introduce a Lagrange parameter α associated with the constraint N, and write the condition for the first variations $\delta S - \alpha \delta N = 0$. Differentiating the expression of the entropy gives $\delta S = -\int (\ln n + 1)\delta n d^2\mathbf{r}$, so that the condition on first variations becomes

$$\int (\ln n + 1 + \alpha)\delta n d^2\mathbf{r} \tag{3.6}$$

This has to be satisfied for any variation δn (function of position) around the optimum state, which is only possible if the term in parenthesis is uniform, so that the density n is uniform: non-interacting particles uniformly mix due to entropy maximization.

- **The mean field approximation:**

Coming back to the interacting particles, a great simplification is provided by the *mean field* approximation, as developed by Joyce and Montgomery in 1973 [52]. The idea is that, due to the long range interactions, each vortex feels the influence of the mean field ψ due to many others, so that we can write the interaction energy with the continuous field expression as

$$E = \frac{1}{2}\int \psi n \gamma d^2\mathbf{r} \tag{3.7}$$

replacing the vorticity ω in (2.16) by the local density $n\gamma$. We suppose first that all the vortices have the same circulation γ, but generalization to several vortex species is straightforward by just adding their contributions to ω. The field ψ is itself given by the Poisson equation (2.7), which becomes $-\Delta\psi = \gamma n$.

The condition on energy brings the new constraint (3.7) for entropy maximization, and a corresponding Lagrange parameter β must be introduced accordingly. Then the condition on first order variations becomes

$$\delta S - \alpha \delta N - \beta \delta E = 0 \tag{3.8}$$

We calculate $\delta E = (\gamma/2)\int(\psi\delta n + n\delta\psi)d^2\mathbf{r}$. In fact the second term is equal to the first, as checked by using the Poisson equation and an integration by parts. The condition on first variations then becomes $\int(\ln n + 1 + \alpha + \beta\gamma\psi)\delta n d^2\mathbf{r}$, which implies that

$$n = n_0 exp(-\beta\gamma\psi) \tag{3.9}$$

(with $n_0 \equiv e^{-\alpha}$). Combining (3.9) and the Poisson equation, we get the self-consistent mean field equation

$$-\Delta\psi = \gamma n_0 exp(-\beta\gamma\psi) \ \ , \ \ \psi = 0 \ on \ boundaries \tag{3.10}$$

Since the locally averaged vorticity $-\Delta\psi$ is a function of ψ, this remarkably represents a steady solution of the Euler equation. A general justification of self-organization into large scale steady flows is thus provided: this is the most probable outcome for the wandering of many small vortices.

The two constants n_0 and β are indirectly given by the constraints on energy and total vortex number. In fact what is given is the product γn_0 (related to the total circulation of the system), while n_0 tends to infinity, and γ tends to 0. The validity of the mean field approximation has been rigorously demonstrated in this limit [36]. Similarly the important parameter is $\beta\gamma$ instead of β, and we can rewrite (3.10) with the non-dimensional variable $\phi = (\gamma n_0)^{-1}\psi$,

$$-\Delta\phi = exp(-B\phi) \ \ , \ \ \phi = 0 \ on \ boundaries \tag{3.11}$$

depending on the single parameter $B = \beta\gamma^2 n_0$.

Note that the expression (3.9) can be obtained in general for a particle in a field with potential energy $\psi\gamma$ in contact with a "thermal" bath with temperature $1/\beta$. This is the so-called canonical approach, in contrast with the micro-canonical approach used her, dealing with an isolated system. These two approaches are generally equivalent, but it is not always so for systems with long range interactions. Note also that some textbooks consider statistical mechanics as the limit of large systems, making the volume goes to infinity. What is important is the limit of a large number of particles, which is here considered in a given domain of finite size. The system is not extensive, on the contrary its spatial confinement is essential.

- **Discussion of results:**

Supposing for instance $\gamma > 0$, it is clear from (3.10) that ψ is a convex function of the coordinates, which is everywhere positive. For positive "temperature" $\beta > 0$, the vorticity tends to be depleted where ψ is maximum, and maximum near the domain boundary, where ψ is set to zero. By contrast for $\beta < 0$, the vorticity tends to be maximum at the vortex center, leading to sharper and sharper maximum of ψ as β is more negative.

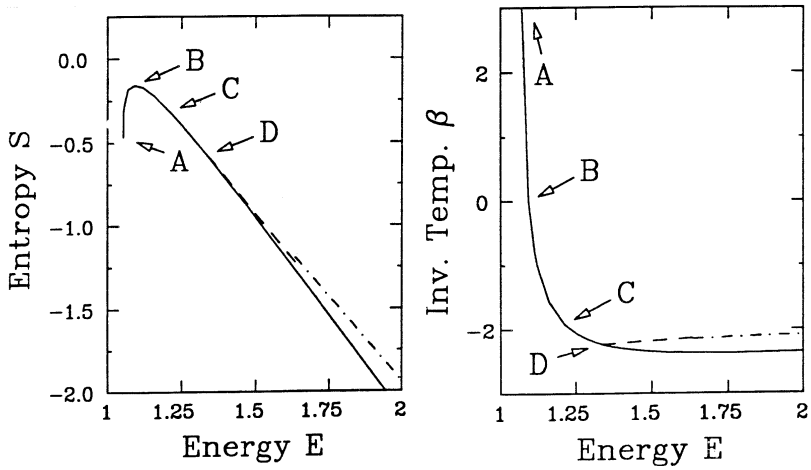

Fig. 7. Entropy (left) and inverse "temperature" $\beta = dE/dS$ (right) versus energy E for the statistical equilibria of a set of N identical point vortices in a disk (from [95]). For small energies (point A) vortices remain near the disk periphery, and the "temperature is positive", while for large energies they remain clumped in a global vortex, more and more concentrated as energy is larger. Then the "temperature" is negative. The entropy maximum (point B) corresponds to a uniform vorticity in the disk, with $\beta = 0$. The solid curves represents axisymmetric equilibria, while the point-dash curve represents a "bifurcated state", in which the vortex spontaneously forms out of the disk axis. This bifurcated state is more likely than the axisymmetric one as it has a higher entropy. It has been indeed observed in a laboratory experiment using a mercury flow in a magnetic field [33]. Note however that, far from boundaries, the axisymmetric equilibrium state is always predicted (the bifurcation is due to the confinement by the disk periphery).

It is interesting to represent the entropy of the statistical equilibrium versus its energy, which has always a bell shape, as shown in Fig. 7. Due to (3.8), the derivative dS/dE (for N fixed) is just β the inverse of the temperature. Therefore the positive temperature is obtained for small energy and negative temperature for large energy. The maximum corresponds to the uniform vortex density: the energy has just the right value to allow for uniform density, which is the state of maximum entropy in the absence of energy constraint, as shown above. Higher energy requires the vortices to remain closely packed, while low energy requires them to remain near

the boundaries. The existence of negative temperature states is forbidden with ordinary particles whose Hamiltonian has a quadratic term in the momentum (the usual kinetic energy): then the entropy always increases with energy. However in the vortex system, such a quadratic term is absent: negative temperature states do occur , and they correspond to the interesting case of clumping of like sign vortices into large coherent vortices.

For several vortex species, with circulation γ_i , the density of each species satisfies a mean field relation (3.9). Then the relationship (3.10) between vorticity and stream function is replaced by a sum of exponentials (or an integral for a continuous distribution of elementary vortex circulation γ,

$$-\Delta\psi = \sum_i \gamma_i n_i exp(-\beta\gamma_i\psi) \quad , \quad \psi = 0 \; on \; boundaries \tag{3.12}$$

For a symmetric set of positive and negative vortices with circulation $\pm\gamma$, we get a sinh function. Note however that symmetry breaking is also possible, so that $n_+ \neq n_-$ even for an equal number of positive and negative vortices. This has been first shown by Pointin and Lundgren, 1976 [84] in a square domain.

In Fig. 8 we show striking examples of symmetry breaking. The statistical equilibrium reached by two initial vortex lines of opposite sign, forming a jet, is considered. The confinement in a channel with periodic boundary conditions is necessary to get an equilibrium. However when the wall is far from the initial jet width d, and the allowed period L sufficiently long, we get an organization with the topology of the Karman vortex street (state DD on the figure). This may explain the observed trend of plane wakes to form such a structure, even in the presence of a strong turbulence (although wakes freely expand with time so they never reach equilibrium). For other parameters shown in Fig. 8, an additional symmetry breaking occurs: vortices on one sign clump together while vortices of opposite sign are dispersed (which favors entropy, while the coherent vortex is necessary to satisfy the energy constraint). The solitary vortex state (SV) qualitatively explains the organization of a turbulent jet observed in an annular channel [100], modeling many dynamical aspects of the Great Red Spot of Jupiter.

- **Limitations:**

The point vortex statistical mechanics explains self-organization. However it does not provide a consistent and quantitative prediction for the Euler system with continuous velocity fields. Of course it is always possible to approximate the continuous velocity fields by a set of many point vortices with a small circulation γ and spacing h , such as $h^2\gamma = \omega$. The limit of small spacing h provides a consistent, stable and convergent approximation [44]. Vortex methods can be used indeed in practice for numerical simulations of

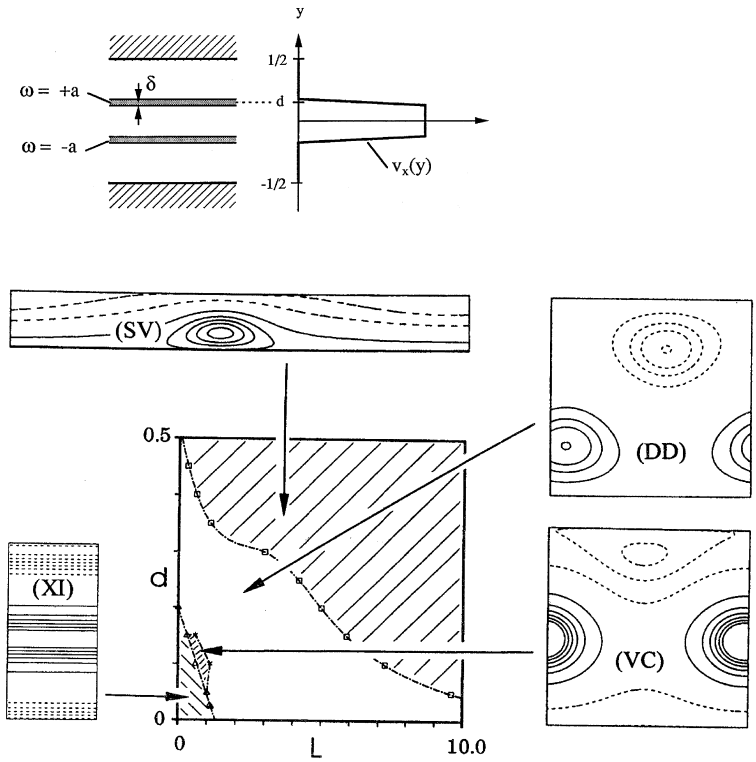

Fig. 8. (from [53]) Statistical equilibria resulting from the mixing of two vortex lines of opposite sign, representing an initial jet in a x-periodic channel, as sketched at the top of the figure. The equilibrium states are represented as a function of the domain length L and the half jet width d (while the channel width is set to unity). The different flow configurations are represented by vorticity isolines for the parameters indicated by the arrows. The boundaries between these configurations are drawn on the diagram. In addition to the x-independent states (XI), we get states breaking the translation symmetry, like the "sinuous mode" (DD). This mode is preferred for small initial jet width d and sufficiently large L, for which the effect of boundary confinement is minimum. For the other states (VC or SV), the additional symmetry breaking between positive and negative vortices is obtained.

the Euler equations [26] [27] [29]. However any approximation to a dynamical system is valid for a finite time, and it may break down for sufficiently long time (which increases with the spatial resolution). The system of N vortices will eventually behave differently from the continuous system, and

the equilibrium statistical mechanics, dealing with the limit of very long times, is different (in more mathematical terms, taking the results of the two limits $h \to 0$ and $t \to \infty$ depends on the order in which they are taken).

There is first the possibility that the maximum vorticity of the statistical equilibrium exceeds the maximum value of the initial condition, which is inconsistent with the Euler equations. Secondly there are several ways to model the same continuous initial condition: we can for instance use either constant vortices with a variable spacing h , or a constant spacing h and different vortex circulations, proportional to the local vorticity. The point vortex statistical equilibrium will be different in the two cases: in the first case we shall get the result (3.10), while in the second case we shall get the result 3.12, with a sum of exponential terms. These difficulties will be solved in section 5 using a different approach.

4 Spectral properties, energy and enstrophy cascade

Since Kolmogorov, the use of spectral representations is at the heart of the study of turbulence. This approach quantifies the energy transfers among the different scales of motion. Kolmogorov's ideas have been applied to 2D turbulence by Kraichnan in 1967 [56], see [58] and [64] for good reviews. The most interesting result is the prediction of an inverse energy cascade toward large scales, whose existence is now firmly established both from numerical simulations and laboratory experiments. The existence of a direct enstrophy cascade toward small scales has been also predicted, but its relevance remains controversial. The emergence of isolated vortices plays an important role, at least in some cases.

4.1 Spectrally truncated equilibrium states:

Instead of using point vortices, a quite different approach is to expand the velocity (and vorticity) field in the eigenmodes ϕ_n of the Laplacian for the fluid domain. These are the Fourier modes for the usual periodic conditions. We therefore expand the vorticity as

$$\omega(t, \mathbf{r}) = \sum a_n(t)\phi_n(\mathbf{r}) \ \ , \ \ with \ \Delta\phi_n = -k_n^2\phi_n \tag{4.1}$$

and the streamfunction is $\psi = \sum a_n k_n^{-2}\phi_n$. Other basis, like wavelets, allow to make scale analysis depending on position, which may be more sensible in the presence of coherent structures, see [39] in this book. However the classical Fourier have the advantage of nice dynamical properties, in addition to their simplicity. In particular each mode ϕ_n is a steady solution of the Euler equations, since its vorticity $-\Delta\phi_n$ is a function of ϕ_n (see section 2.4). The energy E and enstrophy Γ_2 are readily expressed, due to

the orthonormality of the eigenmodes,

$$E = \frac{1}{2}\sum a_n^2 k_n^{-2} \quad , \quad \Gamma_2 = \frac{1}{2}\sum a_n^2 \tag{4.2}$$

Since the Euler equations contain only quadratic terms in velocity, it can be written in the general form

$$\dot{a}_n = \sum_{r,s} A_{nrs} a_r a_s \tag{4.3}$$

with fixed interaction coefficients A_{nrs} for the triad interactions. These coefficients satisfy the "detailed conservation of energy" among each triad

$$k_n^{-2} A_{nrs} + k_r^{-2} A_{rsn} + k_s^{-2} A_{snr} = 0 \tag{4.4}$$

as well as the detailed conservation of enstrophy

$$A_{nrs} + A_{rsn} + A_{snr} = 0 \tag{4.5}$$

Starting with some initial condition with energy limited to a few modes, higher and higher modes will be excited: this is the cascade process of turbulence. It can be understood as a tendency of the system to explore all the available modes, a general effect of entropy increase. However a statistical equilibrium, maximizing entropy, is really reached only if we artificially set a bound to the accessible modes, keeping a finite number N of modes. This stops the fundamental irreversibility of turbulence but gives indications on the general trends of the system.

The spectrally truncated system (4.3) then becomes a closed dynamical system which conserves energy, and the general methods of equilibrium statistical mechanics can be used. Although conservative, it does not have an Hamiltonian form, unlike the vortex system (3.2). Still a Liouville theorem exists

$$\partial \dot{a}_n / \partial a_n = 0 \tag{4.6}$$

which is the required condition for applying statistical mechanics (the volume in phase space is then conserved as mentioned in the footnote of section 3.4). This condition is easily derived: the terms in (4.3) with n, r, s all different give no contribution to $\partial \dot{a}_n / \partial a_n$. The coefficients A_{nss} vanish by the stationary property of the eigenmode ϕ_s. A_{nnn} vanishes in particular, and by (4.4), $A_{nsn} = A_{nns} = 0$. This exhausts the possibilities and we have (4.6).

In the presence of a "thermal bath" with inverse temperature β, the probability of a microscopic state with energy E is in $\exp(-\beta E)$, like we have seen for point vortices in section 3.4. Since there is a second conserved

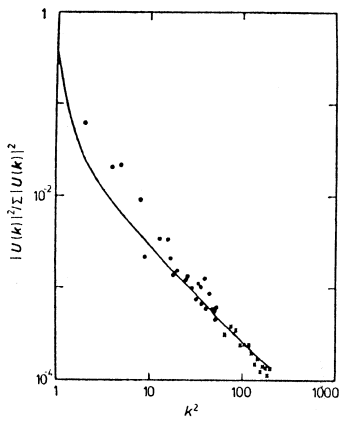

Fig. 9. Normalized modal energies (dots), averaged over 100 time steps, from the numerical solutions of the evolution equations (4.3) for the truncated spectral model, compared to the statistical equilibrium prediction (4.8) in solid line. This run (from [93]) corresponds to a negative β regime with 70 % of the energy condensed in the fundamental mode.

quantity Γ_2, with associated Lagrange multiplyer α, the probability of a state $a_1, ...a_N$ is proportional to $\exp(-\beta E - \alpha\Gamma_2)$. Due to the quadratic expressions (4.2), we have just independent Gaussian probabilities for each mode

$$p(a_n) \propto \exp[-(\beta k_n^{-2} + \alpha)a_n^2/2] \tag{4.7}$$

so the mean energy of a mode is

$$k_n^{-2} < a_n^2 >= k_n^{-2} \int p(a_n)a_n^2 da_n / \int p(a_n)da_n = \frac{1}{2}(\beta + \alpha k_n^2)^{-1} \tag{4.8}$$

For large wavenumbers, it is convenient to the replace the mode number n by the wavevector $\mathbf{k}$, and the discrete mode amplitudes a_n by the Fourier transform $\hat{\omega}(\mathbf{k})$ of the vorticity field. Furthermore the energy spectrum $E(k)$, or the enstrophy spectrum $k^2E(k)$ is used. It is defined by integrating $\hat{\omega}^2(\mathbf{k})$ over a circle with $|\mathbf{k}| = k$, so that for an isotropic field, $k^2E(k) = 2\pi k\hat{\omega}^2(\mathbf{k})$. The total energy is the integral of the energy spectrum, $\mathcal{E} = \int_0^\infty E(k)dk$, and similarly for the enstrophy, $\Gamma_2 = \int_0^\infty k^2E(k)dk$. The equilibrium spectrum is therefore in $k/(\beta + \alpha k^2)$.

For 3D turbulence, we have only the conservation of energy, so that $\alpha = 0$, and the energy is equally spread over the modes. This is not in agreement with actual turbulence, but it justifies the tendency of energy to spread over all the accessible modes, and therefore to undergo an energy cascade toward the small scales where a majority of modes is located. In

contrast for 2D turbulence we can have a variety of states, depending on β and α, which can be indirectly related to the mean energy and enstrophy of the system. A particularly interesting case corresponds to $\beta \to -\alpha k_0^2$ for which the energy can accumulate in the lowest available mode k_0, as represented in Fig. 9. This figure also indicates that the statistical mechanics prediction is well verified by numerical computations of the dynamical system (4.3), artificially truncated by keeping a finite number of modes without dissipation.

This helps to understand the self-organization into the lowest mode, with a model different from that of point vortices. The artificial truncation of high modes have then little influence. Note however that the truncation suppresses conservation laws (2.11) other than enstrophy. Moreover the use of a canonical distribution is then questionable, as energy is concentrated in the single lowest mode, with large fluctuations. For instance the most probable state corresponds to the center of the Gaussian (4.7), with zero energy. The use of a micro-canonical approach, keeping the energy constant, would lead to a different and more realistic result, although the trend for concentration in the lowest mode should be the same.

4.2 The enstrophy and inverse energy cascades of forced turbulence:

- **The double cascade of Kraichnan(1967)**

In the absence of confinement at small wavenumbers (e.g. boundaries) and artificial cutoff at high wavenumbers the cascades can freely develop. To study stationary regimes, it is convenient to consider a statistically permanent forcing concentrated at a given wavenumber k_I. The dimensional analysis leading to the Kolmogorov cascade can be carried out in 2D as well as in 3D and it yields the same inertial range,

$$E(k) = C\epsilon^{2/3}k^{-5/3} \tag{4.9}$$

The direction of the energy flux is not given by dimensional analysis. However a direct cascade toward high wave numbers is forbidden by the absence of energy dissipation (see 2.3). Therefore Kraichnan suggested a cascade toward large scales (small k). He further justifies this cascade direction as a trend of the system to go toward the statistical equilibrium described above (although it never reaches it in the absence of spectral truncation). There is no need for energy dissipation at large scales, at least in the ideal case of an infinite fluid domain, since the integral $\int k^{-5/3}dk$ diverges at 0: energy progressively accumulates toward lower and lower k. More physically, we shall see that a friction force proportional to the velocity (Rayleigh friction) can progressively pump out the energy along the inverse cascade.

Now what happens toward the small scales? Enstrophy must be injected by the forcing, at a rate $\eta = k_I^2\epsilon$, where k_I is the injection wavenumber.

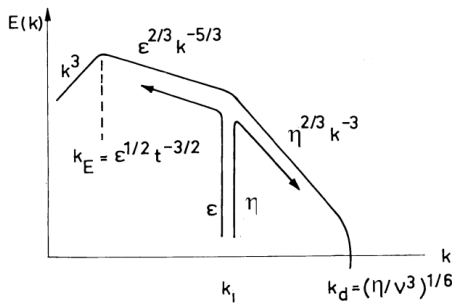

Fig. 10. sketch of the classical double cascade of 2D turbulence (from Lesieur [64]).

Then an enstrophy cascade is expected, which can be predicted by dimensional analysis in the same way as the energy cascade, just replacing energy by enstrophy, and ϵ by η. This yields an energy spectrum

$$E(k) = C'\eta^{2/3}k^{-3} \tag{4.10}$$

We shall see that these two cascades are mutually exclusive (for infinitely extended cascades): the rate of enstrophy transfer vanishes in the energy cascade and the rate of energy transfer vanishes in the enstrophy cascade. Therefore since energy goes to the larger scales, the enstrophy cascade must be toward small scales. Enstrophy can be dissipated at small scales by viscosity unlike energy. Even without viscosity the enstrophy cascade can theoretically extends with time to higher and higher wavenumbers. Fig. 10 summarizes this theoretical double cascading spectrum.

For a more precise discussion of these cascade processes, let us express the forcing as a vorticity source $f(x, y, t)$ added on the right hand side of (2.6), and introduce some energy dissipation. Then the mode enstrophies $< a_n^2 >$ satisfy the equations

$$\frac{1}{2}\frac{d < a_n^2 >}{dt} =< a_n \dot{a}_n >= \sum_{r,s} A_{nrs} < a_r a_s a_n > + < f_n a_n > -diss \tag{4.11}$$

where f_n is the amplitude of f in the mode n. Note that the enstrophy production is the correlation $< f_n a_n >$ between the vorticity and its source f, and the corresponding energy production $k_n^{-2} < f_n a_n >$. The sums of these quantities over the modes are the total enstrophy production η and energy production ϵ respectively.

For the considered homogeneous isotropic turbulence, the discrete mode amplitudes a_n is replaced by the Fourier transform $\hat{\omega}(\mathbf{k})$, and the energy

equation (4.11) takes the form of a conservation equation for the energy spectrum$E(k)$,

$$\frac{\partial E}{\partial t} = -\frac{\partial \Pi}{\partial k} + \ forcing \ - \ diss \tag{4.12}$$

Π can be viewed as the energy flux due to nonlinear interactions and $\partial\Pi/\partial k$ its divergence. The same equation can be also written in a form displaying enstrophy conservation

$$k^2\frac{\partial E}{\partial t} = -\frac{\partial Z}{\partial k} + \ forcing \ - \ diss \tag{4.13}$$

with an enstrophy flux Z. These fluxes are explicitly obtained [56] [64] by Fourier transform of the Euler equations and integration over wavevector directions. They are expressed as integral of the rates of triad energy transfer $T(k,p,q)$, depending on the triple correlations $< \hat{\omega}(\mathbf{k})\hat{\omega}(\mathbf{p})\hat{\omega}(\mathbf{q}) >$, where the vectors $(\mathbf{k},\mathbf{p},\mathbf{q})$ form a triangle $(\mathbf{k}+\mathbf{p}+\mathbf{q}=0)$ with sides k,p,q,

$$\Pi(k) = \frac{1}{2}\int_k^\infty dk' \int_0^k T(k',p,q)dpdq \ - \ \frac{1}{2}\int_0^k dk' \int_k^\infty T(k',p,q)dpdq \tag{4.14}$$

$$Z(k) = \frac{1}{2}\int_k^\infty k'^2dk' \int_0^k T(k',p,q)dpdq \ - \ \frac{1}{2}\int_0^k k'^2dk' \int_k^\infty T(k',p,q)dpdq \tag{4.15}$$

At this stage a possible approach is to introduce a closure hypothesis to express the triple correlations and obtain dynamical equations for the energy spectrum. This has been done by assuming that the fluctuations of the mode amplitudes have statistics close to a Gaussian. After a failed attempt by Millionshtchikov (the quasi-normal theory), this approach has been widely developed by Kraichnan. His models have the property of relaxing the system toward the spectrally truncated statistical equilibrium in the absence of forcing and dissipation. With forcing at a given wavenumber k_I, these closure models lead to the double cascade sketched in Fig. 10 [3] [49], see [64]for a review.

However Kraichnan did not use closure hypothesis in his original paper of 1967. He assumes instead an infinite cascade, with forcing and dissipation replaced by constant flux in wavenumber space. He further assumes that the transfer rate $T(k,p,q)$ scales in power law: $T(k,p,q) = k^{-m}T(1,p/k,q/k)$, where $T(1,p/k,q/k)$ depends only on the angles in the triad. Then the energy flux (4.14) is expressed as k^{3-m} (due to the triple integrals) multiplied by angular integrals over triad directions p/k and q/k. The only possibility for a flux $\Pi(k)$ independent of k is therefore $m=3$. By dimensional analysis, $T(k,p,q) \sim u^3/k^2$, where u is the typical velocity at scale $1/k$, and $E(k) \sim u^2/k$. Therefore, $T \sim k^{-3}$ implies $u \sim k^{-1/3}$, corresponding to an

energy spectrum in $k^{-5/3}$. This dimensional analysis is however valid only if the triple correlations scale in u^3 while the double correlations scale in u^2, i.e in the absence of intermittency. The cascade is more fundamentally defined by the scaling of the transfer rate than the scaling of the energy spectrum (double correlations).

Such constant energy flux cascades can be as well obtained in 3D, but in 2D one can furthermore imagine cascades with a constant enstrophy flux $Z(k)$, corresponding to the k^{-3} energy spectrum. Then the energy flux $\Pi(k)$ should scale in k^{-2}. However by using the detail conservation laws (4.4) and (4.5), which translate into similar relations for $T(k,p,q)$, Kraichnan shows that the angular integration in (4.14) exactly cancels: the energy flux is zero. Similarly the enstrophy flux cancels in the energy cascade. As stressed by Kraichnan, a cascade cannot be viewed just as a carrying belt in wavenumber space, transporting together the energy $E(k)$ and its related enstrophy $k^2E(k)$. The transport is rather the result of overlapping triads, which makes possible a flux of energy or enstrophy alone. Eyink [35] has obtained mathematical results supporting this double cascade theory. He has shown that the flux of higher vorticity moments, e.g. ω^4 is related to the enstrophy cascade and is also toward high wavenumbers.

This work of Kraichnan provides constraints on the nature of putative cascades, but it does not guarantee that such states should be approached. As mentioned above, closure models provide a first support of these ideas. The enstrophy cascade has received a more precise theoretical justification by a different approach [37], presented at the same school [38]. The idea is derived from the study of the passive scalar stirring in a random large scale strain. Batchelor in 1959 first predicted k^{-1} spectra for the scalar variance, and this has been confirmed by rigorous approaches. Vorticity in 2D turbulence is transported like a scalar, and we notice that the k^{-3} energy spectrum corresponds indeed to a k^{-1} enstrophy spectrum [57]. Of course the strain is not limited to large scales: the strain produced by flow structures at scale k^{-1} can be estimated as $uk \sim (k^3E(k))^{1/2}$. This strain is independent of k for a k^{-3} energy spectrum so the contribution of all scales is the same, and the "nonlocal interactions" with the large scale strain is dominant (unlike in the $k^{-5/3}$ spectrum), but only marginally. The precise analysis [37] gives a k^{-3} energy spectrum corrected by a logarithmic factor. Kraichnan also proposed [57] such a logarithmic correction to avoid some divergence in the calculations.

- **Observations of the cascades:**

It is difficult to simultaneously observe the two cascades due to the required spatial resolution and high Reynolds number: observing two decades for each cascade in a numerical computation would require at least 10^4 grid points in each direction. Simulations or laboratory experiments must be

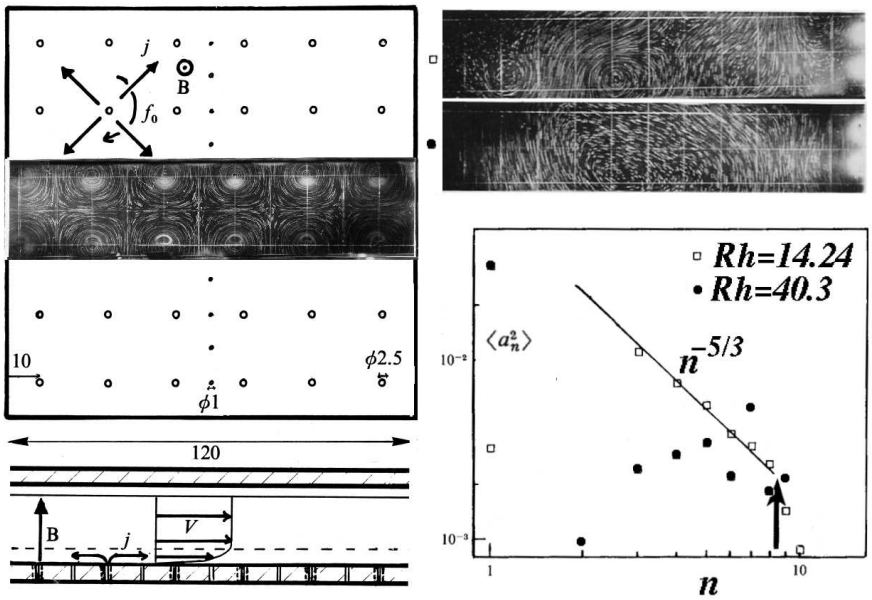

Fig. 11. Laboratory observation of the inverse energy cascade, from [97]. The experimental cell is sketched on the left as a top view and side view below. The flow is maintained 2D in a horizontal mercury layer by a vertical magnetic field which prevents the built up of 3D perturbations. The electric current, steadily injected with alternating sign in an electrode lattice, generates a square vortex lattice by interaction with the magnetic field. The flow is visualized from above by the streaks of particles floating on the mercury free surface (the field of view is limited to a central band due to the constraint of the electromagnet). The dynamics is controlled by a friction parameter Rh representing the ratio of the inertial effect to the friction on the bottom surface. For Rh <1.78, the flow is steady as shown on the left, over the apparatus sketch. For higher Rh instabilities develop, exciting larger scales of motion, as shown on the two photos on the right top. The corresponding energy spectra reveal the built up of an inverse energy cascade for $Rh = 14.24$, and the condensation in the fundamental mode $n = 1$ for $Rh = 40.3$. This mode corresponds to a global rotation of the flow, spontaneously breaking the symmetry between positive and negative vorticity. The spectra are obtained from the spatial Fourier transform of the electric potential measured along a line of small electrodes ($\emptyset$ 1): the induced electric potential is proportional to the transverse velocity.

optimized to study one of the cascades.

The existence of the inverse energy cascade is now well established both from direct numerical simulations [42] [96] and from laboratory ex-

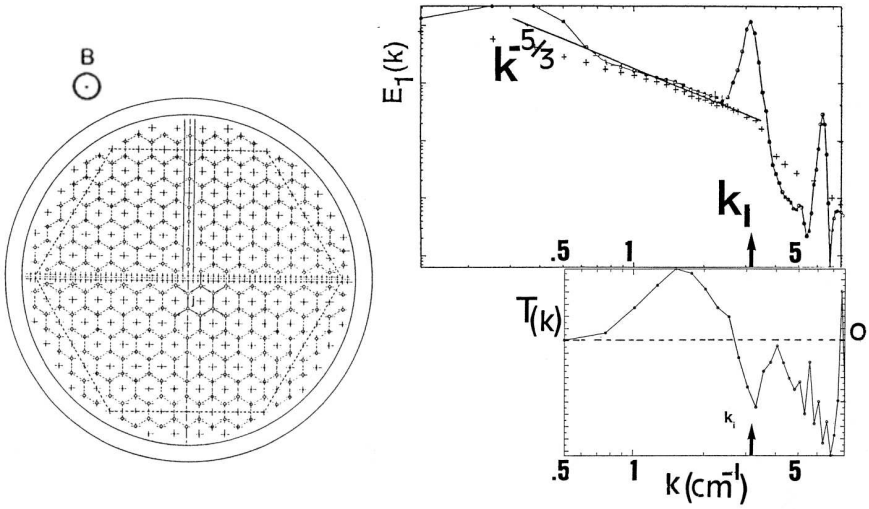

Fig. 12. Forcing 2D turbulence with the same technique as in Fig. 11, but with an hexagonal lattice (from [76]). The energy spectra indicate a persistent peak at the forcing wavenumber, which is removed if the mean velocity is subtracted from the data, keeping only the turbulent part with a hint of a $k^{-5/3}$ range. The spectral energy transfer $\mathcal{T}(k) = -d\Pi/dk$ have been also obtained from the triple velocity correlations, assuming isotropy. One checks that the energy transfer indeed feeds the small wavenumbers while it removes energy from the forcing range.

periments [97] [76] [83]. Note that the experiments of Sommeria [97] have been performed with a steady forcing (in a square vortex lattice), and the inverse cascade is therefore spontaneously generated, see Fig. 11. Spontaneous generation of an inverse energy cascade has been also observed with an hexagonal lattice, see Fig. 12, although a significant steady flow component coexists with the turbulence, unlike with the square lattice, more efficient at generating 2D turbulence (see also section 3.3). In contrast, both the experiments of Paret and Tabeling [83] and the numerical simulations have been performed with some random forcing. The Kolmogorov constant found is about 7, which means that this cascade is less "efficient" than in 3D (for which $C = 1.5$): for a given value of the spectrum $E(k)$ the transfer rate ϵ is smaller than in 3D. Notice that this value of the coefficient fits well with the prediction of Kraichnan using the test field closure model [57].

Remarkably, intermittency seems absent [83] [96], or at least very weak: the successive moments of the two-point velocity difference $< (\delta\mathbf{u})^n >$ scale with point separation r in $r^{n/3}$. The ideas of Kolmogorov (1941) turns out to be more appropriate for 2D than for 3D turbulence! Furthermore the probability distribution for $\delta\mathbf{u}$ is close to a Gaussian at all scales. It cannot

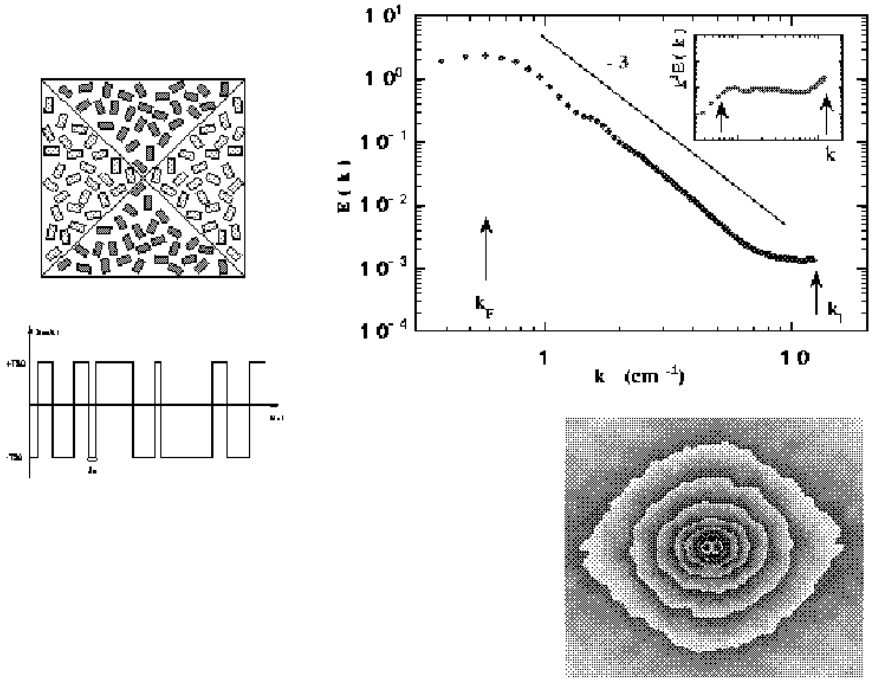

Fig. 13. Laboratory observation of the direct enstrophy cascade in a thin water layer, stratified in density by salinity to restrict 3D recirculation (from [82]). The flow is generated by a set of magnets (sketch on the upper left) interacting with a uniform horizontal electric current randomly switched in time (curve below). The flow is thus generated at large scale allowing to focus the study on the enstrophy cascade. Spectra in k^{-3} are indeed obtained (upper right), while the spectral isocontours below illustrate the isotropy of the cascade, although the forcing at small k is not isotropic, as revealed by the two peaks near the center.

be exactly a Gaussian as the energy transfer is associated with a non zero third order moment, as seen above. However the cascade is less efficient than in 3D (the Kolmogorov constant is larger) so we can understand that the system is closer to an equilibrium with Gaussian statistics.

To get a steady cascade in a finite size domain, some energy dissipation acting at large scale is necessary. In laboratory experiments the friction on the support of the fluid layer, proportional to velocity, plays this role. In numerical simulations, a large scale dissipation consistent with the inverse energy cascade must be chosen [101]. When the inverse cascade is limited by the domain size instead, the cascade breaks down and condensation of energy in the lowest mode is obtained as predicted above from truncated

spectral equilibria. This condensation has been well observed both in laboratory experiments [97] [83] (see Fig. 11) and numerical computations [96].

The existence of the enstrophy cascade is also confirmed by laboratory experiments [82], represented in Fig. 13. Note that measurements of the steep k^{-3} energy spectra over large wavenumber ranges is difficult as it requires a very high precision to distinguish the small scale fluctuations from the much stronger large scales (obtaining two decades requires a precision on velocity better than 10^{-3}). Numerical simulations with high resolution [5], up to 4096^2 provide more extended spectral ranges, with a constant enstrophy flux over 2 decades. The k^{-3} energy spectrum has logarithmic corrections, while a nearly perfect k^{-3} spectrum has been obtained with a slightly different forcing [67]. Note that earlier simulations [63] point out that the presence of coherent vortices modifies the cascade, leading to steeper energy spectra. The permanent production of random vorticity tends however to prevent the build up of the coherent vortices [5], unlike in freely decaying flows discussed next.

4.3 The enstrophy cascade of freely evolving turbulence:

Unlike in 3D, the behavior of freely evolving 2D turbulence is quite different than that of forced turbulence. This difference can be understood by considering that the dynamical time for eddies with scale k^{-1} is in $(k^3E(k))^{-1/2}$, so that in a $k^{-5/3}$ energy spectrum the small scales have a much shorter dynamical time than the large scales (it is in $k^{-2/3}$). Therefore in a direct energy cascade the effect of large scales is reasonably similar to a permanent forcing for the smaller scales. This is not true for the effect of small scales on the large scales in the inverse energy cascade.

A classical prediction for a freely evolving turbulence have been given by Batchelor in 1969, assuming a self-similar spectral evolution, with a (single) time scale and length scale evolving in time. An enstrophy cascade is still predicted, with a spectrum in $t^{-2}k^{-3}$. The inverse energy cascade is then replaced by a growth of the integral scale, such that the total enstrophy is predicted to decay in t^{-2}.

Energy spectra close to k^{-3} are indeed obtained in laboratory experiments or numerical simulations of freely decaying 2D turbulence. Experimentally, it has been first measured in grid turbulence in liquid metal duct flows submitted to a transverse magnetic field [55]. This was the first experimental observation of 2D turbulence ever reported. Recent measurements in soap films yield similar results [71]. Numerical simulations starting with some random field at wavenumber k_I first show the onset of a k^{-3} energy spectral range, when the enstrophy dissipation is maximum [9] [8]. However the spectra tend to become progressively steeper as isolated vortices form, see below.

Numerical simulations [16], as well as laboratory experiments [102], all

indicate that enstrophy decays much less rapidly than the Batchelor's prediction in t^{-2} (the exponent found in various cases is in the range 0.3-1 instead of 2). This global decay is related to the spectral behavior in the limit of small wavenumbers. Recent numerical simulations [80] allowing a good resolution at small wavenumber confirms a behavior in k^3 predicted with closure models [3]. This probably depends however on assumptions on the initial condition [32]. In laboratory experiments such large scales are clearly less universal, and more difficult to control than the small scale behavior.

4.4 The emergence and evolution of isolated vortices:

The emergence of isolated vortices is a fascinating aspect of 2D turbulence. This phenomenon has been first documented by Mc Williams [107], and then obtained in many similar numerical computations. Most vortices are monopoles but some dipoles, and even tripoles, can be temporarily formed. Such vortex formation has been observed as well in laboratory experiments with thin water layer [102] and more spectacularly in electron plasma experiments [40], where the vorticity field is directly visualized as electron density. This organization can be explained in terms of statistical mechanics, see section 5, as a local equilibrium around an initial vorticity maximum.

Once formed these vortices interact and merge, so they become fewer and fewer, while their maximum vorticity only weakly decays. Therefore they dominate more and more the background vorticity, which decays by enstrophy cascade. Note that some contour dynamics computations [34] indicate the possibility of formation of new secondary vortices of various sizes by the reorganization of vorticity filaments resulting from vortex interactions. Persistence of non-axisymmetric vortices is also observed in such computations. These results are however not supported by electron plasma experiments [75], as well as more classical numerical computations with increasing resolution [8]: significant vortex formation only occurs during the initial stage of organization from the random initial condition. Statistical mechanics also indicates a general trend for merging and reorganization into axisymmetric vortices.

The formation of organized vortices has a clear consequence in terms of global statistics. In particular the Kurtosis $Ku =< \omega^4 > / < \omega^2 >^2$ considerably increases with time: it is just the inverse of the area proportion occupied by the vortices. Starting from a value Ku =3 characterizing the Gaussian statistics of the initial condition, a typical value of Ku =50 can be reached, which characterizes a highly intermittent field: the distribution of vorticity levels has big "tails" corresponding to a significant probability of finding vorticity values much larger than the vorticity root mean square. Steepening of the energy spectrum beyond the k^{-3} prediction is also observed to be associated with vortex predominance, while k^{-3} spectra are

observed in regions outside the vortices [39].

The condition of formation of such organized vortices is still a debated question. They are best observed for an initial condition spectrum with a dominant peak, while a wideband range of scales (like a $k^{-5/3}$ inertial range) tends to prevent their formation. The conditions at large scales seem to have a significant influence. The effect of the dissipation operator at small scale is also important: the classically used hyperviscous operators can spuriously enhance the vortex influence (the peak vorticity can increase), while the usual viscosity makes then wider. "Contour surgery" methods lead to different results as mentioned above. Well tested high resolution numerical studies are still needed to make safe claims about the asymptotic inertial limit, in particular about the statistical distribution of vortex strength and size.

The evolution of the vortex population is an interesting theoretical issue. At moderate Reynolds numbers, the vortices have all a similar size and strength. At higher Reynolds numbers, vortices with different sizes coexist, but their probability distribution seems to reach a steady shape [8], so that further evolution is controlled in all cases by an increase of the typical vortex radius r_a and a decrease of the vortex number N. Power law evolutions $N \propto t^{-\xi}$ and $r_a \propto t^{\xi/4}$are observed for these quantities, while the typical peak vorticity remains constant. The relation between the exponent for vortex radius and vortex number is justified by the conservation of energy. This indeed implies the conservation of the typical flow velocity, which is induced by the vortices with a scaling in γ/l, where $\gamma \propto r_a^2$ is the vortex circulation and $l \propto N^{-1/2}$ is the typical vortex separation. Therefore a constant typical velocity indeed implies that $Nr_a^4 \propto const$. The total vortex area $Nr_a^2 \propto t^{-\xi/2}$, then decreases with time, so that some vorticity is mixed away in the background during merging. Since enstrophy becomes dominated by the vortices, this total vortex area is just proportional to the enstrophy.

An exponent $\xi \simeq 0.7$ is obtained in direct numerical simulations [8] and laboratory experiments [102], and it is reproduced by a model of "punctuated dynamics" [14]: a set of N point vortices interact according to the Kirchhoff equations (3.2,3.3), and a merging rule is used when two vortices get closer than their radius. Such a model has been recently improved [94] using a procedure of "numerical renormalization" to reach much longer evolution times: after each merging, the domain of computation is increased, introducing randomly a new vortex to keep the same vortex density. This allows to keep a constant vortex number in the computations, while previous methods required a very large initial vortex number to get good statistics at later times. These calculations agree with the previous ones at early times, but a progressive increase of the exponent ξ is observed, with a final value $\xi = 1$.

This final value can be understood by an elementary kinetic model, considering vortices like atoms in ballistic motion. The rate of binary collisions is then proportional to the square $N^2 \propto t^{-2\xi}$ of the vortex density, to the vortex size $r_a \propto t^{\xi/4}$ (its cross-section of interaction) and to the constant vortex velocity. This would imply $dN/dt \propto t^{-(7/4)\xi}$ so that $\xi = 4/3$, clearly inconsistent with the results. However Sire and Chavanis [94] show that three-body collisions are necessary to get merging. Typically a vortex dipole (two opposite sign vortices) with separation $\propto r_a$ collides with a monopole. In that case the pair translates at velocity $\gamma/r_a \propto r_a$. Assuming uncorrelated random pair formation, the density of dipoles is $\propto N \times N r_a^2$ (the vortex density multiplied by the probability of finding another vortex at a distance $\propto r_a$). The collision probability therefore becomes $dN/dt \propto N \times N^2 r_a^2 \times r_a \times r_a$ (the successive product of the vortex density, the dipole density, the collision cross section r_a, and the dipole velocity). This yields the exponent $\xi = 1$.

This work therefore clarifies the problem of punctuated vortex dynamics. Its practical relevance for 2D turbulence is however remote, as it is limited to very large time scales and domain sizes, with accordingly extremely high Reynolds numbers. Furthermore the question of energy spectra is open. Assuming random uncorrelated point vortices completely determines in principle the statistics of the velocity field [20]. In particular the energy spectrum is [78] in k^{-1} for $k > 1/l$, where l is the typical distance between vortices (this can be understood by remarking that the Fourier transform of a Dirac function is constant, leading to an enstrophy spectrum in k). Therefore some correlations between vortex positions must occur to explain the steeper spectra numerically observed. Statistical mechanics of point vortices, beyond the mean field approximation discussed in section 3.4, should be relevant there.

5 Equilibrium statistical mechanics and self-organization

5.1 Statistical mechanics of non-singular vorticity fields:

We have seen in subsection 3.4 that the statistical mechanics of point vortices explains self-organization of 2D turbulence into large steady coherent structures. However we have noted that the modeling of continuous flows by point vortices leads to some difficulties. A solution to this problem has been proposed by Kuz'min(1982), rediscovered and justified by Robert [85], Robert & Sommeria [88], and independently by Miller [74]. This equilibrium statistical theory is performed directly on the Euler equations.[5]Then,

[5]A similar statistical mechanics had been previously proposed [68] for the Vlasov equation used to describe the organization of galaxies with stellar dynamics. The analogies with the Euler equations have been put forward only recently [25] [18]

the standard procedure for Hamiltonian systems of particles is not available, but the method is still justified (on a weaker basis) by a set of rigorous properties [90]. The result is again a steady solution of the Euler equations, on which fine scale vorticity fluctuations are superimposed. The relationship between vorticity and streamfunction is different that of the point vortex model, and it is now quite consistent with the properties of the Euler equations with nonsingular vorticity.

- **The macroscopic description:**

The Euler equations are known to develop very complex vorticity filaments, at finer and finer scales, and a deterministic ("microscopic") description of the flow would require a rapidly increasing amount of information as time goes on. We are rather interested in some local vorticity average $\overline{\omega}$. However to keep track of the conservation laws, we need to introduce a more precise "macroscopic" description, as the probability $\rho(\mathbf{r}, \sigma)$ of finding the vorticity level σ in a small neighborhood of the position $\mathbf{r}$ (this is a Young's measure in mathematical terms). The locally averaged vorticity field is then expressed in terms of this probability density as:

$$\overline{\omega}(\mathbf{r}) = \int \rho(\mathbf{r}, \sigma)\sigma d\sigma \tag{5.1}$$

This probability can be viewed as the local area proportion occupied by each vorticity level σ, and it must satisfy at each point the normalization condition :

$$\int \rho(\mathbf{r}, \sigma) d\sigma = 1 \tag{5.2}$$

and the associated (macroscopic) stream function satisfies in the fluid domain $(\mathcal{D})$:

$$\overline{\omega} = -\Delta\psi \quad \text{with} \quad \psi = 0 \quad \text{on} \quad (\partial\mathcal{D}) \tag{5.3}$$

Note that since the streamfunction is expressed by space integrals of vorticity, it smoothes out the local vorticity fluctuations, supposed at very fine scale, so ψ has negligible fluctuations.

It is then possible to express the conserved quantities as integrals of the macroscopic fields. A first set of conserved quantities is the global probability distribution of vorticity $\gamma(\sigma)$ (i.e. the total area of each vorticity level):

$$\gamma(\sigma) = \int \rho(\mathbf{r}, \sigma) d^2\mathbf{r} \tag{5.4}$$

As a consequence the integral of any function of the vorticity is conserved (the vorticity elements are just rearranged within the bounded fluid domain as time goes on).

The energy (2.16) is also conserved. As discussed above the streamfunction can be considered as smooth, so we can express the energy in terms of the locally averaged vorticity:

$$E = \frac{1}{2} \int \psi \overline{\omega} d^2\mathbf{r} \tag{5.5}$$

In a domain with rotational or translational symmetries, additional quantities are conserved like the angular momentum in the disk, as discussed in section 2.3.

- **Entropy maximization:**

As in usual statistical mechanics, for instance in section 3.4, we need to determine the entropy ("counting" the associated microscopic states) of a given macroscopic state. The macroscopic state which maximizes the entropy, with the constraint of the conserved quantities, will be the most likely to result from complex stirring. The expression of the entropy is the usual mixing entropy,

$$S = -\int \rho(\mathbf{r}, \sigma) \ln \rho(\mathbf{r}, \sigma) d^2\mathbf{r} d\sigma \tag{5.6}$$

The difference with point vortices lies in the local normalization condition (5.2): we count the possible rearrangements of small vorticity parcels which exclude each other on a given area unlike point vortices.[6]

We therefore maximize the entropy with the constraints (5.4), (5.5) and (5.2) due to the conserved quantities and to the normalization. This variational problem is treated by introducing the corresponding Lagrange multipliers β, $\alpha(\sigma)$, $\zeta(\sigma)$ so that the first variations satisfy:

$$\delta S - \beta \delta E - \int \alpha(\sigma) \delta\gamma(\sigma) d\sigma - \int \zeta(\mathbf{r}) \delta \left(\int \rho(\mathbf{r}, \sigma) d\sigma \right) d^2\mathbf{r} = 0 \tag{5.7}$$

By analogy with usual thermodynamics, β can be viewed as the inverse temperature and $\alpha(\sigma)$ the chemical potential of species σ. Introducing the expressions (5.6) and (5.5) of entropy and energy, (5.7) becomes $\int [\ln \rho + 1 + \alpha(\sigma) + \zeta(\mathbf{r}) + \beta\sigma\psi]\, \delta\rho\, d^2\mathbf{r} d\sigma = 0$. This has to be satisfied for any variation $\delta\rho$, implying that the integrand vanishes. The resulting optimal probability density $\rho(\mathbf{r}, \sigma)$ is therefore related to the equilibrium streamfunction ψ by the relationship:

$$\rho(\mathbf{r}, \sigma) = \frac{1}{Z} g(\sigma) e^{-\beta\sigma\psi} \tag{5.8}$$

[6] This entropy can be further justified by considering the system as the limit of a series of spectrally truncated approximations of increasing resolution [90].

where $g(\sigma) \equiv e^{-\alpha(\sigma)}$ and $Z \equiv e^{\zeta(\mathbf{r})}$.

This is like in the case of point vortices, the vorticity level σ replacing the elementary vortex circulation γ. However the additional normalization constraint (5.2) has to be satisfied at each point, which leads to :

$$Z(\psi) = \int g(\sigma) e^{-\beta\sigma\psi} d\sigma \tag{5.9}$$

so that Z is a function of ψ, which we call the partition function by analogy with usual statistical mechanics. The locally averaged vorticity (5.1) is then expressed as a function of the streamfunction:

$$\overline{\omega} = \frac{\int g(\sigma)\sigma e^{-\beta\sigma\psi} d\sigma}{\int g(\sigma) e^{-\beta\sigma\psi} d\sigma} = -\frac{1}{\beta Z}\frac{\partial \ln Z}{\partial \psi} \equiv f_{\beta,g}(\psi) \tag{5.10}$$

and the resulting flow can be calculated by solving the corresponding partial differential equation:

$$-\Delta\psi = f_{\beta,g}(\psi) \quad \text{with} \quad \psi = 0 \quad \text{on} \quad (\partial\mathcal{D}) \tag{5.11}$$

Like in the point vortex case, random mixing yields a steady solution of the Euler equations once the local vorticity fluctuations have been averaged.

The parameters β and $g(\sigma)$ are indirectly determined by the conservation laws, and we call the resulting solutions of (5.11) the Gibbs states. This is only a necessary condition for a true statistical equilibrium: in addition the second variation of the entropy must be negative. A good way to select such maxima is to use a relaxation algorithm which increases the entropy while preserving the conserved quantities. The relaxation equations of section 6 fulfil this goal, provided an appropriate discretization is implemented. A relaxation algorithm in discrete steps has been also implemented [106].

5.2 The Gibbs states:

- **Case of vortex patches:**

In the case of an initial condition made of patches with vorticity 0 or a, we can write ρ in terms of the Dirac distribution δ as $\rho(\sigma, \mathbf{r}) = p(\mathbf{r})\delta_{(\sigma-a)} + (1-p(\mathbf{r}))\delta_{(\sigma)}$ involving the local area proportion $p(\mathbf{r})$ of the level a and the complementary $1-p$ for the level 0. Then the result (5.11) reduces to

$$-\Delta\psi = pa = a\frac{e^{-\beta a\psi}}{g_0 + e^{-\beta a\psi}} \quad \text{with} \quad \psi = 0 \quad \text{on} \quad (\partial\mathcal{D}) \tag{5.12}$$

Making a formal analogy with quantum gas statistics, this can be called a Fermi-Dirac distribution by contrast with the Boltzmann relation (3.10) for point vortex statistics. Similarly the local exclusion of the vorticity

patches results in a saturation of the vorticity at the unmixed value a, when $\exp(-\beta a\psi) \gg g_0$. In the opposite limit, the relation (5.12) reduces to the point vortex result (3.10). We call it the dilute limit [88] as it corresponds to a small initial vorticity area which has been diluted among the dominant irrotational fluid.

For practical calculations in the more general case, the initial vorticity field has to be discretized in vorticity levels, so that the function $f_{\beta,g}$ can be expressed by sums of exponential terms at both numerator and denominator. The result generally converges already well when just a few levels are used.

An example of statistical equilibria is represented in Fig. 14. The geometry is a channel, with periodic boundary conditions along x (which can be viewed as a simplified representation of an annulus). The mixing of a single level vorticity patch with a given initial area A is considered (here A =1/10 of the total surface). The accessible energy is then restricted between a lower and an upper bound. At the lower bound, the vorticity is pushed to the walls, without any possibility of mixing, so the entropy remains equal to zero. At the upper bound, mixing is also forbidden, and the vorticity forms a central patch. This state breaks the translational symmetry. The branch of x-independent states has lower entropy and is not a maximum beyond the bifurcation (it is numerically obtained by suppressing all x-dependent perturbation). The entropy versus energy has a bell shape curve, whose slope is the inverse temperature β, equal to $+\infty$ at the low energy bound and to $-\infty$ at the high energy bound. Between these two bounds, the entropy reaches a maximum with $\beta = 0$, corresponding to a complete mixing, with a uniform coarse grained vorticity.

The point vortex mean field equilibrium is obtained from the present result by taking the limit of a small area A (for a fixed energy). An explicit family of solutions is then available in this channel geometry: the Stuart vortices [98]. This point vortex statistics leads to a similar bell shaped curve (like in Fig. 7), but without energy bound: the vortices can concentrate without limit, in contradiction with the conservation of the maximum vorticity.

Note that for negative temperature states, the equilibrium structure is self-confined along the transverse direction by energy conservation. The lateral walls have no influence (unlike in the jet case with zero global circulation represented in Fig. 8). In contrast the x wise periodicity sets the scale of the bifurcated vortex state. The Gibbs state equation (5.12) has also solutions with smaller x-wise periods, but they are not entropy maxima: the largest scale is always preferred, which justifies the tendency for vortex merging and growth of the free shear layer.

- **General properties of the Gibbs states:**

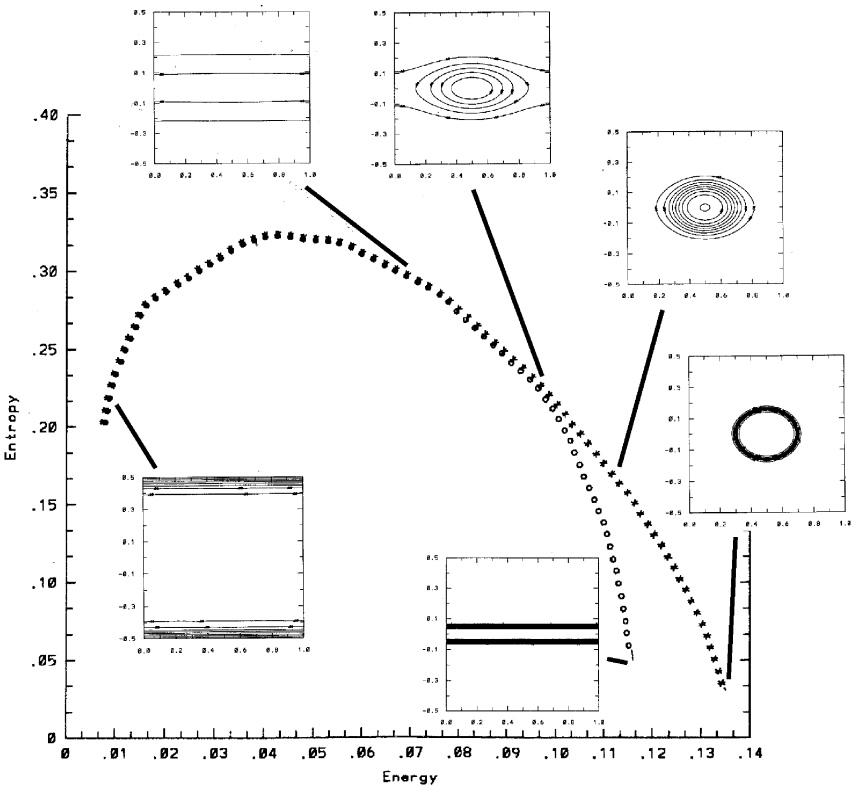

Fig. 14. Statistical equilibrium for an initial single level vorticity patch in a channel with periodic conditions along x (from [106]). The entropy is plotted versus energy, and representative vorticity fields $\overline{\omega}$ are given (isovorticity contours). For sufficiently high energy, vorticity clumps in a large vortex, breaking the translational symmetry.

For any global distribution $\gamma(\sigma)$ of vorticity levels, the accessible energy is restricted between a lower and an upper bound [13]. At the upper bound, any vorticity mixing is forbidden, and the entropy remains equal to zero, with an inverse temperature $\beta = -\infty$. The behavior at the lower bound depends on the total circulation Γ. For a non-zero circulation, the entropy versus energy has a bell shape curve, as in Fig. 14. At its maximum, $\beta = 0$, the coarse grained vorticity is uniform. With $\Gamma = 0$, a state of zero energy can be reached, with complete mixing, $\overline{\omega} = 0$, so the entropy is maximum for $E = 0$. It decreases with increasing energy, so the inverse temperature β is always negative. This is the case for instance in a doubly periodic

domain, for which $\Gamma = 0$ by construction.

General properties of the function $f_{\beta,g}$ can be shown [88]. First of all it is always bounded between the minimum and maximum values of the initial vorticity, which is expected since the vorticity $\overline{\omega}$ results from a *mixing* of the vorticity levels. Secondly $f_{\beta,g}$ is always a monotonic function of ψ. This is most easily shown by differentiating the expression (5.10) of $f_{\beta,g}$, which yields an expression for the local enstrophy[7]

$$\omega_2 \equiv \overline{\omega^2} - \overline{\omega}^2 = \frac{\int g(\sigma)\sigma^2 e^{-\beta\sigma\psi} d\sigma}{\int g(\sigma) e^{-\beta\sigma\psi} d\sigma} - (\frac{\int g(\sigma)\sigma e^{-\beta\sigma\psi} d\sigma}{\int g(\sigma) e^{-\beta\sigma\psi} d\sigma})^2 = -\frac{1}{\beta} f'_{\beta\, g}(\psi) \tag{5.13}$$

Since $\omega_2 \geq 0$, the derivative $f'_{\beta,g}$ is of the sign opposite to β : $f_{\beta,g}$ is an increasing function for negative temperature and a decreasing function for positive temperature.

It can be shown [88] that the Gibbs state equation (5.11) has a unique solution for β larger than a negative bound, so there is no bifurcation, in particular for $\beta > 0$. The Gibbs state is then nonlinearly stable in the sense of Arnold. In practice stability is observed in all cases for the maximum entropy states, but there is no available demonstration in the presence of bifurcation. The statistical equilibria are also stable in all cases with respect to further mixing [88] : if we smooth out the fluctuations, taking $\overline{\omega}$ as the new initial state, the final state remains unmixed.

***Linearized cases and minimum enstrophy:**

Near the maximum of the entropy versus energy, $\beta \simeq 0$, so one can linearize the function $f_{\beta,g}$, and (5.11) becomes a linear (Helmholtz) equation. This "limit of strong mixing" provides nice possibilities for analytical results and classification of the bifurcations [21] [23]. Furthermore, the Gibbs state then depends only on the normalized energy E/Γ_2 and circulation $\Gamma/\Gamma_2^{1/2}$. Expansion of $f_{\beta\, g}$ in powers of ψ can be performed, and each successive term depends on successive higher moments of the vorticity. Therefore the statistical equilibrium for strong mixing does not depend on the detail distribution of the vorticity levels (only on the normalized energy and circulation), but it becomes more and more dependent as the mixing is prevented by energy conservation.

There is also a different possibility for obtaining a linear relationship $f_{\beta\, g}$ between vorticity and streamfunction. It corresponds to a Gaussian function $g(\sigma)$, as easily checked by substitution in (5.10). It corresponds to a particular distribution of vorticity levels $\gamma(\sigma)$, which depends on the energy.

[7] This can be viewed as a relation between fluctuations and polarizability, like in magnetism [24]. Similarly the successive moments are related to the successive higher derivatives of $f_{\beta,g}$ [12].

A linear relationship between vorticity and streamfunction is also obtained by a principle of "minimum enstrophy" [62] or "selective decay" [45]. The rational is that the enstrophy decays in the limit of small viscosity, while energy, and possibly other robust integrals like the angular momentum, remain constant. Then a natural idea is that the system evolves until it minimizes its enstrophy for a given energy (and possibly other constraints). This yields a linear relationship between vorticity and stream function. This prediction is good in some cases, but not of general validity. For instance in the case of electron plasma, with vorticity always positive (proportional to the electron density), this can yield spurious negative vorticity, in the absence of an additional constraint [11]. The point of view of the statistical theory is that part of the initial enstrophy Γ_2 is irreversibly transferred into fine grained (microscopic) vorticity fluctuations, so that the final coarse grained enstrophy $\Gamma_2^{c.g} = (1/2)\int \overline{\omega}^2 d^2\mathbf{r}$ is always smaller than Γ_2,

$$\Gamma_2^{c.g} \equiv \frac{1}{2}\int \overline{\omega}^2 d^2\mathbf{r} = \frac{1}{2}\int \overline{\omega^2} d^2\mathbf{r} - \frac{1}{2}\int (\overline{\omega^2} - \overline{\omega}^2) d^2\mathbf{r} < \Gamma_2 \tag{5.14}$$

However $\Gamma_2^{c.g}$ is truly minimized only in the linearized cases. In conclusion, a minimum enstrophy principle appears as a particular limit of entropy maximization, either in the limit of strong mixing either in the Gaussian case (see [21] for details).

5.3 Tests and discussion:

A first test of the statistical mechanics predictions is shown in Fig. 15 by comparison with numerical simulations of the Navier-Stokes equations at low viscosity. The shear flow in a channel with periodic boundary conditions develops vortices which self-organize in a steady flow after complex evolution. When plotted on a scatter-plot of the vorticity versus streamfunction, the points of the field collapse on a curve, confirming that the flow approaches a steady solution of the Euler equations (although a slow decay persists due the small viscosity). The global flow structure indeed corresponds to what is predicted by statistical mechanics, as shown in Fig. 14. Moreover, a linear relationship is obtained in the vortex core between $ln[\omega/(a-\omega)]$ and ψ, where a is the vorticity of the initial vorticity strip. This linearity is equivalent to (5.12). We observe however that the agreement is limited to the region of active stirring and that little mixing occurs outside. As a consequence, the maximum vorticity remains a little larger than predicted.

Similar results have been obtained for the usual vortex merging [33]. For a jet in a channel, the states (DD) and (VC) predicted in Fig. 8 have been remarkably checked by numerical simulations [53]. In a laboratory experiment, the organization into a single vortex by merging of a few initial vortices has been correctly predicted, while discrepancy progressively

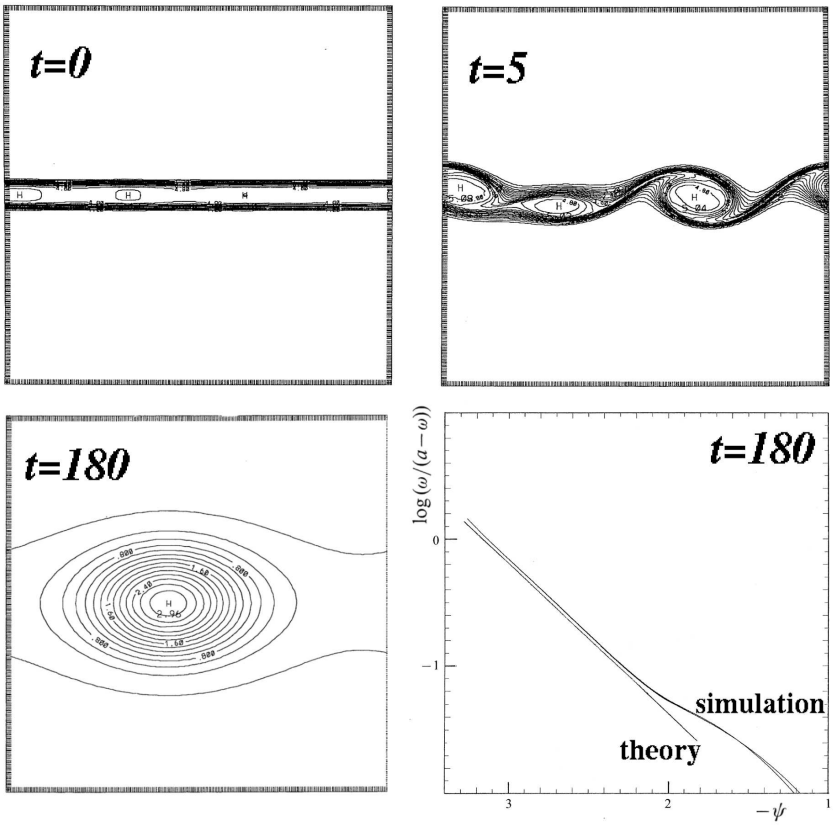

Fig. 15. Test of the statistical mechanics prediction (5.12) from direct numerical simulations of the Navier-Stokes equations (from [98]).

arises after successive merging events [70]. Similar conclusions arise from comparisons with simulations of turbulence in a periodic domain [10].

An explanation of this discrepancy is that viscosity modifies the distribution of vorticity levels in zones of strong strain. Under the effect of a strain s, we can estimate that the scale η of a vorticity structure exponentially decreases $\eta = \eta_0 \exp(-st)$, until smoothing occurs by viscous diffusion. This happens when the diffusion time η^2/ν equals the straining time s^{-1}, so that $\eta_0^2 \exp(-2st) = \nu/s$. Estimating $s \sim U/L$ and $\eta_0 \sim L$ from the large scale L and typical velocity U, we find that viscosity is influent after a time $t = (2s)^{-1} \ln Re$, which increases only logarithmically with the Reynolds number Re. In contrast the time for reaching the statistical equilibrium is controlled by vorticity, so that the prediction will be good only in zones

where vorticity dominates strain, in the vortex core. The range of validity of the statistical theory is expected to improve with increasing Re, but only logarithmically.

Capel and Pasmanter [12] have recently proposed a model to take into account the modification of vorticity levels by a weak viscosity. In a different attempt, Turkington [105] has proposed to keep only the vorticity extrema as conserved quantities in the statistical theory, instead of the whole distribution of vorticity levels. Finally, Chavanis and Sommeria [23] have introduced the concept of "restricted statistical equilibrium", maximizing entropy in a "bag" with free boundaries. It is assumed isolated from the outside irrotational flow by kinetic restriction to mixing, due to vanishing fluctuations (see next section). The organization into steady dipoles, like observed in Fig. 5, can be explained by this method. Entropy maximization would indeed make the dipole spread to infinity in the absence of restriction (while the monopoles are self-confined by energy conservation).

In laboratory experiments, boundary layer detachment can bring vorticity in the fluid interior and consequently modify the statistical equilibrium. This effect is striking in spin-up experiments in a rectangular container [47].

The formation of vortex lattices in an electron plasma disk [40] seems also in contradiction with the statistical theory: calculations with a single non-zero vorticity level predict merging in a single vortex. However, if the vortices are taken as given objects, their interaction with the background vorticity is remarkably described by statistical mechanics: both the lattice geometry and the density field in the background are quantitatively accounted [51]. These vortex lattice are probably meta-stable equilibrium states (local entropy maxima) with three vorticity levels: 0, an intermediate level in the background and the strong vortex cores. A slight change in the initial condition makes them organize in the main equilibrium state with a single vortex.

In conclusion, although various restrictions can prevent reaching the true statistical equilibrium, complex stirring clearly tends to increase the entropy, whose expression (5.6) is supported by many arguments. This will be used in next section to model the evolution of 2D turbulence.

6 Eddy diffusivity and sub-grid scale modeling

6.1 Thermodynamic approach:

Diffusion processes are classically considered as a relaxation toward statistical equilibrium. The linear non-equilibrium thermodynamics states that the fluxes driving the system toward equilibrium are proportional to the gradient of the thermodynamic "potentials", for instance species concentration. We use a similar idea [89], expressed by means of a "Maximum Entropy Production" (MEP) principle, to drive eddy fluxes for 2D turbulence. The goal

is two-fold: to compute the statistical equilibrium corresponding to a given initial condition, and to propose a subgrid-scale modelling for computations of the actual flow evolution with coarse resolution (LES).

Like for equilibrium states, the flow is described in terms of a local probability $\rho(\mathbf{r},\sigma)$ of vorticity levels σ at position $\mathbf{r}$. However this probability is now assumed to evolve with time. The conservation of vorticity levels is written in terms of a transport equation for ρ, by both the explicit velocity $\mathbf{u}$ and an eddy flux $\mathcal{J}$ due to the subgrid-scales:

$$\partial_t\rho + \mathbf{u}.\nabla\rho = -\nabla.\mathcal{J} \ \ , \ \ with\ \mathcal{J}.\mathbf{n} = 0 \ \ , \ \ on\ \partial\mathcal{D} \tag{6.1}$$

At the wall the normal eddy flux $\mathcal{J}.\mathbf{n}$ must vanish due to impermeability. The explicit velocity $\mathbf{u}$ derives from the streamfunction ψ by (2.5), and its curl is equal to $\overline{\omega}$, related to the field ρ by

$$-\Delta\psi = \overline{\omega} = \int \sigma\rho\, d\sigma \ , \ with\ \psi = 0\ on\ \partial\mathcal{D} \tag{6.2}$$

We can deduce from (6.1) an equation for the locally averaged vorticity $\overline{\omega}$ by integration over the vorticity levels σ,

$$\partial_t\overline{\omega} + \mathbf{u}.\nabla\overline{\omega} = -\nabla.\mathcal{J}_\omega \tag{6.3}$$

where we have introduced the vorticity flux

$$\mathcal{J}_\omega = \int \sigma\mathcal{J}\, d\sigma \tag{6.4}$$

We are mostly interested in the field $\overline{\omega}$, as the local fluctuations are in practice sensitive to viscous effects, but we cannot directly close (6.3) and, like for equilibrium states, we need to work with the probabilities ρ, solving the equations (6.1) .

Of course we first need to determine the flux $\mathcal{J}$. We first express the rate of entropy increase, by time differentiating (5.6), expressing $\partial_t\rho$ by (6.1), and noting that $\rho\ln\rho$ is conserved by the advective term,

$$\dot{S} = -\int \mathcal{J}.\nabla(\ln\rho)\ d^2\mathbf{r}d\sigma \tag{6.5}$$

In order to relax toward statistical equilibrium, the entropy must clearly increase with time.

In fact we determine $\mathcal{J}$ such that, for a given field ρ at each time t, $\mathcal{J}$ *maximizes* the entropy production $\dot{S}$, with the appropriate dynamical constrains, which are:

-the conservation of the local normalization (5.2), implying

$$\int \mathcal{J}\, d\sigma = 0 \tag{6.6}$$

-the energy conservation expressed from (5.5) and (6.3) as

$$\dot{E} = \int \mathcal{J}.\nabla\psi d^2\mathbf{r} = 0 \tag{6.7}$$

- a limitation on the eddy flux $\mathcal{J}$, characterized by a bound $C(\mathbf{r})$, which exists but is not specified.

$$\int \frac{\mathcal{J}^2}{2\rho} d\sigma \leq C(\mathbf{r}) \tag{6.8}$$

A justification of this choice is that the quantity $\mathcal{J}/\rho$ can be considered as the velocity producing the flux $\mathcal{J}$, so the integral $\int \rho(\mathcal{J}/\rho)^2 d\sigma$ is the total energy of this diffusion velocity, a natural quantity to bound. Another justification is that it yields results consistent with the classical approach of linear non-equilibrium thermodynamics [89].

This variational problem is treated by introducing (at each time t) Lagrange multipliers, denoted $\zeta(\mathbf{r}), \beta, 1/A_E$ for the three respective constraints. It can be shown by a convexity argument that reaching the bound (6.8) is always favorable for increasing $\dot{S}$, so that this constraint can be replaced by an equality. Therefore the condition

$$\delta\dot{S} \; - \; \int \zeta(\mathbf{r})\delta\mathcal{J} \; d^2\mathbf{r}d\sigma \; - \; \beta\delta\dot{E} \; + \; \int \frac{1}{A_E(\mathbf{r})}\frac{\delta\mathcal{J}^2}{2\rho} \; d^2\mathbf{r}d\sigma \; = \; 0 \tag{6.9}$$

must be satisfied for any variations $\delta\mathcal{J}(\sigma\,\mathbf{r})$, which yields

$$\mathcal{J} \; = \; -A_E(\mathbf{r},t) \; [\nabla\rho + \beta\rho(\sigma - \overline{\omega})\nabla\psi]. \tag{6.10}$$

The Lagrange multiplier $\zeta(\mathbf{r})$ has been eliminated, using the condition (6.6) of local normalization conservation.

The first term in the eddy flux (6.10) represents a usual diffusion: the flux of the quantity ρ is proportional to its gradient. The second term states that vorticity diffusion is constrained by the energy conservation of the induced flow: vorticity is not a passive quantity. Remembering the analogy of ψ with an interaction potential, this second term can be called a drift term, with a flux proportional to the "force" $\nabla\psi$, like sedimentation in a gravitational field.

At equilibrium, the flux must vanish, so the drift term balances diffusion. One can check that this yields again the Gibbs state (5.8), with β the corresponding inverse "temperature". During flow evolution this quantity varies and is determined by the condition of energy conservation. Introducing (6.10) in the condition (6.7) of energy conservation, we indeed obtain,

$$\beta = -\frac{\int A_E(\nabla\overline{\omega}).(\nabla\psi)d^2\mathbf{r}}{\int A_E(\nabla\psi)^2\omega_2 d^2\mathbf{r}} \tag{6.11}$$

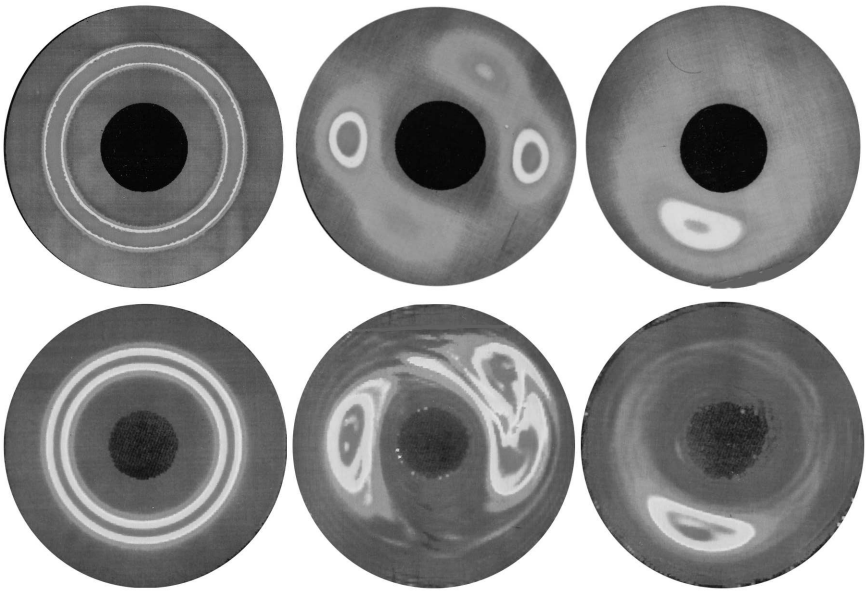

Fig. 16. Instability and final organization of a vorticity strip in an annular channel (at three successive times from left to right). The relaxation model (top), with low resolution (4000 grid points), is from T. Dumont, Laboratoire d'Analyse Numrique, Univ. Lyon. It is compared with a direct numerical simulation [69] (bottom).

where $\omega_2 \equiv \overline{\omega^2} - \overline{\omega}^2 \equiv \int \sigma^2 \rho d\sigma - (\int \sigma \rho d\sigma)^2$ is the local enstrophy.

We have thus obtained a complete set of dynamical equations (6.1,6.2), (6.10,6.11), which exactly conserves the distribution of vorticity levels and energy. This system relaxes to statistical equilibrium at an optimum rate. We can express the entropy production (6.5) as $\dot{S} = \int \mathcal{J}^2 (A_E \rho)^{-1} d^2\mathbf{r} d\sigma$ so the eddy diffusivity A_E must be *positive* to satisfy the condition of entropy increase. Except for its sign, the diffusivity is not determined by this thermodynamic approach: it is related to the unknown bound (6.8) on the flux.

These relaxations equations are suitable to calculate the statistical equilibrium resulting from any initial condition. Once numerically implemented, it provides a convenient way to solve the Gibbs state equation (5.8) with the appropriate constraints. Furthermore it selects an entropy *maximum* among these solutions, since it is obtained by an entropy increase.[8]

[8] It can be proved that stable steady solutions of the relaxation equations are indeed entropy maxima (P.H. Chavanis, in preparation)

For practical implementation, the simplest case is the evolution of vorticity patches with only one non-zero vorticity level $\sigma = a$. Then we have only one equation (6.1), and the vorticity is proportional to this density, $\overline{\omega} = \rho a$. Fig. 16 shows an example of the evolution of a vortex ring in an annulus, compared with a high resolution numerical simulation of the same process. Although the relaxation equation smooths out the local vorticity fluctuations, it correctly handles the large scale dynamics. Moreover the final vortex remains in its statistical equilibrium, without any further diffusion. Comparisons with direct numerical simulations (DNS) in various cases, with both positive and negative vorticity patches (formation of dipoles and tripoles) show good agreement [86].

For general initial conditions, one has to discretize the vorticity levels σ (in practice good convergence is already obtained with a few levels). The vorticity flux can be directly calculated by integration of (6.10) over the vorticity levels, $\mathcal{J}_\omega = -A_E(\mathbf{r},t)\ [\nabla\overline{\omega} + \beta\omega_2\nabla\psi]$, but the local enstrophy ω_2 itself depends on the transport of the probability distribution ρ. An eddy flux of momentum, in $A_E(\mathbf{r},t)\ [\nabla^2\mathbf{u} - \beta\omega_2\mathbf{u}]$, is also associated [24].

These relaxation equations have the advantage of being fully consistent with the properties of the Euler equations, and the comparison with DNS is quite good. While their justification by the MEP principle is somewhat philosophical, a more precise justification has been obtained by kinetic approaches, discussed in next section. These approaches provide estimates of the diffusion coefficient A_E, and justify the presence of the drift term, but they also stress some limitations.

Other limitations can be seen from the structure of the equations themselves. A first difficulty is that the constraint of energy conservation is only global. This is reasonable, due to the long range vortex interactions, but in a very large domain we expect that two sub-systems will evolve independently. The integral condition (6.11) should be replaced by a more local condition (the temperature should not remain uniform but diffuse with time toward an equilibrium). Furthermore the equations are not invariant by a change of reference frame, which is again problematic in a large domain. The MEP has been extended [22] to solve all these difficulties, but the model is more complex and has not been numerically implemented. Furthermore it involves additional unknown diffusivity coefficients for energy and momentum.

6.2 Kinetic models

The relaxation equations were justified in previous section by thermodynamical arguments, without discussing the mechanisms. Further insight has been recently provided by kinetic models inspired from the analogies with stellar systems and plasma physics [18].

A first approach is provided by the point vortex model, which has the

advantage of fitting in the standard framework for N-body statistical mechanics. The vortices are assumed randomly positioned with the density close to the mean field statistical equilibrium. Each vortex diffuses by the random close encounters with the other vortices. Moreover each vortex induces a velocity field (added to the dominant mean field) which systematically displaces all the other vortices in its neighborhood. Chavanis [17] finds that the induced displacement (like a polarization effect in electrostatics) reacts back on the considered vortex. It results in a drift, in $-A_E\beta\sigma\nabla\psi$, explaining the second term in the flux 6.10 (in the diluted case $\sigma \gg \overline{\omega}$ for which the point vortex approximation applies). At negative temperatures, the drift tends to attract together like-sign vortices, and its effect exactly balances diffusion at equilibrium. Both effects are proportional to the same coefficient A_E which can be explicitly calculated. Such a correspondence between the drift coefficient (friction) and diffusion is quite general, it is similar to the Einstein formula for the Brownian motion[9].

Coming back to non-singular vorticity fields, we can classically make a decomposition of the Euler vorticity equation (2.6) into explicit and implicit parts, $\omega = \overline{\omega} + \tilde{\omega}$. We assume that $\overline{\omega}$ is an ensemble average, which therefore commutes with the spatial derivatives. In particular a fluctuating velocity $\tilde{\mathbf{u}}(\mathbf{r}) = \int \tilde{\omega}(\mathbf{r}')\mathbf{K}(\mathbf{r}-\mathbf{r}')d^2\mathbf{r}'$ is induced by these fluctuations, where the Kernel $\mathbf{K}(\mathbf{r}-\mathbf{r}')$ expresses the velocity induced at point $\mathbf{r}$ by a unit singular vortex at position $\mathbf{r}'$, $\mathbf{K}(\mathbf{r}-\mathbf{r}') = (1/2\pi)\mathbf{e_z} \times (\mathbf{r}-\mathbf{r}')/|\mathbf{r}-\mathbf{r}'|^2$ plus the effect of the image vortices near the boundary). Assuming fluctuations with a short (Lagrangian) correlation time τ_c, the diffusion coefficient is classically given as $A_E = (1/4)\tau_c\overline{\tilde{\mathbf{u}}^2}$ (Taylor, 1921). From the previous expression of $\tilde{\mathbf{u}}$, we get

$$\overline{\tilde{\mathbf{u}}^2} = \int \overline{\tilde{\omega}(\mathbf{r}')\tilde{\omega}(\mathbf{r}'')}\mathbf{K}(\mathbf{r}-\mathbf{r}').\mathbf{K}(\mathbf{r}-\mathbf{r}')d^2\mathbf{r}' \tag{6.12}$$

Assuming a short correlation length ϵ for the vorticity, $\overline{\tilde{\omega}(\mathbf{r}')\tilde{\omega}(\mathbf{r}'')} = \epsilon^2\overline{\tilde{\omega}(\mathbf{r}')^2}\delta(\mathbf{r}'-\mathbf{r}'')$, we can write a local approximation of (6.12), assuming $\overline{\tilde{\omega}(\mathbf{r}')^2} \simeq \overline{\tilde{\omega}(\mathbf{r})^2}$, $\overline{\tilde{\mathbf{u}}(\mathbf{r})^2} = \epsilon^2\overline{\tilde{\omega}(\mathbf{r})^2}\int_\epsilon^L (2\pi r')^{-1}dr'$. We find that the vorticity fluctuations at all scales contribute equally to the local velocity fluctuations, and we have arbitrarily cut the integral between ϵ and the domain scale L. Nevertheless the result, in $\ln(L/\epsilon)$, depends only weakly on these bounds, so the local approximation yields a reasonable estimation,

$$A_E = \frac{\tau_c\epsilon^2}{8\pi}\ln(\frac{L}{\epsilon})\overline{\tilde{\omega}^2} \tag{6.13}$$

The diffusivity is proportional to the local enstrophy $\omega_2 \equiv \overline{\tilde{\omega}^2}$ and increases with the scale ϵ, typically the cutoff scale. The correlation time τ_c

[9] In this diluted case $\sigma \gg \overline{\omega}$ (or point vortex statistics), the relaxation equations are equivalent to Fokker-Planck equations describing diffusion with drift in a potential ψ

can be estimated as $\omega_2^{-1/2}$, the time scale of the local fluctuations, or as the inverse of the strain rate of the explicit flow. Both times are of the same order as the global time scales, so that the short correlation is only marginally justified, like the local approximation made above. In any case, the diffusivity vanishes for weak local enstrophy fluctuations ω_2. This explains to some extent the existence of the "restricted statistical equilibria" mentioned above: relaxation toward equilibrium is efficient inside the active region but weak mixing occurs at the periphery, due to the vanishing of the vorticity fluctuations.

Chavanis [19] has proposed a more precise analysis, which furthermore provides the drift term in addition to diffusion. He starts from the equations

$$\partial_t \overline{\omega} + \mathcal{L}\overline{\omega} = -\nabla.\overline{\widetilde{\mathbf{u}}\widetilde{\omega}} \ , \quad with \ \mathcal{L} \equiv \overline{\mathbf{u}}.\nabla \tag{6.14}$$

$$\partial_t \widetilde{\omega} + \mathcal{L}\widetilde{\omega} = -\widetilde{\mathbf{u}}\nabla\overline{\omega} \tag{6.15}$$

similar to the quasi-linear approximation made in plasma physics. The first one is the classical Reynolds averaged Euler equation (2.6), with an eddy flux $\mathcal{J} = \overline{\widetilde{\mathbf{u}}\widetilde{\omega}}$. The second one is the equation for the fluctuations $\widetilde{\omega} = \omega - \overline{\omega}$, neglecting two terms,$-\widetilde{\mathbf{u}}\nabla\widetilde{\omega}$ and $\overline{\widetilde{\mathbf{u}}\nabla\widetilde{\omega}}$, assumed of weak influence on $\overline{\omega}$. In contrast $\widetilde{\mathbf{u}}\nabla\overline{\omega}$ builds up the eddy flux with a term $\partial_t\overline{\widetilde{\mathbf{u}}\widetilde{\omega}} = \overline{\widetilde{\mathbf{u}}^2}\nabla\overline{\omega}$ producing diffusion in (6.14).

Assuming again a delta-correlated vorticity field, Chavanis [19] finds an eddy flux and a drift term as integrals over the Lagrangian trajectories of the explicit flow $\overline{\omega}$. Quite remarkably, the resulting kinetic equation satisfies a H-theorem: the entropy (5.6) always increases with time. This result provides a new, independent, support of the statistical equilibrium approach. The expressions of the flux are in general non-local in time and space. They reduce to the local flux (6.10) only close to equilibrium. Therefore, the relaxation equations obtained by the thermodynamic approach provide the right tends, but are probably of limited accuracy to describe the flow evolution.

The initial hypothesis of random fluctuations is not easily justified, in contrast with 3D turbulence. Some simulations suggest that the implicit scales are mostly strained by the large scales, which suggests to defined $\overline{\omega}$ as a filtered field rather than an ensemble average. Then new terms appear [61] in (6.14) and (6.15). Nevertheless, on longer time scales, chaos should develop and the probabilist approach may be more appropriate to capture the long time trends of the system.

7 Conclusions:

Our knowledge of 2D turbulence has made great progress in the last ten years, due in particular to the availability of high resolution computations.

Fig. 17. Wake behind a knife blade in a soap film, the flow comes from the left, (from M. Rutgers, 1996 (http://www.physics.ohio-state.edu/~maarten).

Simulations at resolution 4096^2 are now currently available, and simulations at resolution 512^2, which were at the forefront of research ten years ago, are accessible on a good home computer. In spite of this great progress, with a growing consensus on some aspects, many results are still under debate. There is a need for careful computations at still higher resolution, comparing various numerical methods, initial and forcing conditions. One possible reason for the observed discrepancy may be that truly asymptotic results, forgetting the details of the initial conditions, require a very long time and high Reynolds numbers. The results on punctuated vortex dynamics discussed in section 4.4 support this point of view.

Nevertheless some robust results are obtained in laboratory experiments. Many results of 2D turbulence seem to be remarkably insensitive to weak 3D perturbations, which are always present to some extent. The availability of various laboratory experiments has been a strong motivation for the recent rise of interest and progress in 2D turbulence.

The course has been focused on two fundamental aspects, the spectral cascades and the self-organization into coherent structures. The double-cascade theory of Kraichnan has received a remarkable confirmation by experiments and simulations. A new approach [38], adapting field theoretical methods developed for the passive scalar, brings a rigorous support to the

enstrophy cascade forced by random large scale motion. Concerning the inverse cascade, the quasi-Gaussian statistics raises also hope for a deeper theoretical insight. In contrast with the forced case, the freely decaying turbulence progressively deviates from the classical enstrophy cascade law, as coherent vortices emerge and become more and more isolated, increasing the intermittency. The statistics and kinetics of this vortex system represents challenging problems of current interest.

The self-organization into coherent structures is well explained by statistical mechanics of vorticity. This theory provides good predictions in cases of rapid stirring, checked in both numerical simulations and laboratory experiments. Although various limitations can prevent the system for reaching true equilibrium, it still reveals the trends of the evolution. This provides new ideas for developing LES adapted to the peculiar properties of 2D turbulence. It supports the use of an ordinary (positive) eddy viscosity, whose energy dissipation is compensated by a drift term, acting at large scale. At statistical equilibrium these two terms balance each other. These results have been recently further justified in terms of kinetic models, but the diffusion flux and drift appear in general as integrals over space and previous times, rather than local effects.

Many questions about 2D turbulence have been left aside. The problem of predictability is for instance of great interest for applications to the atmosphere, see e. g. [64] for a discussion using closure models. Lorenz first addressed this question with severely truncated spectral models, the only models accessible to simulation at that time, and found his famous "butterfly" effect: the exponential growth of errors associated with chaos in low dimensional systems. However when all the degrees of freedom are recovered, a new regularity occurs, of statistical nature, as illustrated by the formation of organized structures at statistical equilibrium. Then the butterfly effect disappears [87].

The transport of a scalar is another important subject not discussed in this course, but with active recent theoretical progress both in 3D and 2D (see [38]). In fact most results and questions in usual turbulence have a counterpart in 2D, for instance in the classical shear flow problems. Channel or plane boundary layer flows are stable in the 2D case. By contrast the boundary layer detachment, with Kelvin-Helmholtz instability and vortex roll-up is basically a 2D process. Its analogy with decaying homogeneous 2D turbulence has been stressed [65]. Jets or wakes tend to organize in dipoles [31], and Fig.17 shows the fascinating structure of the wake behind a knife in a soap film. Understanding the role of these coherent structures in the global statistics of these 2D flows may be helpful for the 3D cases.

Many results in 2D turbulence can be relevant to a rotating and density stratified medium, like occurring in atmosphere, oceans, and even protoplanetary disks [7]. The statistical mechanics approaches of section 5 and 6

have been extended to the quasi-geostrophic model [50] [73] [99], with application to the Great Red Spot of Jupiter [6]. Extension to the more general shallow water system [24] can be readily applied to multilayer (isopycnal) models used in oceanography.

One should finally note the fascinating analogies with different physical systems. We have seen above that an electron plasma in a magnetic field satisfy the 2D Euler equations. A neutral plasma can be described by more complex 2D models, in analogy with some geostrophic planetary flow problems. The Vlasov equation, for plasma or stellar systems, has also formal analogies [25] [18] with the Euler equation, but in the 6D phase space rather than in 2D. These analogies are further motivations to better understand 2D turbulence.

References

[1] H. Aref, "Integrable, chaotic, and turbulent vortex motion in two-dimensional flows", Ann. Rev. Fuid Mech. 15, 345-89, 1983.

[2] C. Bardos "Existence et unicité de la solution de l'équation d'Euler en dimension deux", J. Math. Anal. Appl. 40, 769-790, 1972.

[3] C. Basdevant, M. Lesieur and R. Sadourny, "Subgrid scale modelling of enstrophy transfer in two-dimensional turbulence", J. Atmos. Sci. 35, 1028-1042, 1978.

[4] G. K. Batchelor, "An introduction to fluid dynamics", Cambridge University Press, 1967.

[5] V. Borue, "Spectral exponents of enstrophy cascade in stationary two-dimensional homogeneous turbulence", Phys. Rev. Letters 71 (24), 1993.

[6] F. Bouchet and J. Sommeria, "Emergence of intense jets and Jupiter Great Red Spot as maximum entropy structures", submitted to J. Fluid Mech. (e-print physics/0003079).

[7] A. Bracco, P. H. Chavanis, A. Provenzale and E. Spiegel "Particle aggregation in a turbulent Keplerian flow" Phys. Fluids 11, 2280-2286, 1999.

[8] A. Bracco, J.C. McWilliams, G. Murante, A. Provenzale and J.B. Weiss, "Revisiting freely decaying two-dimensional turbulence at millenium resolution", Phys. Fluids 12 (11), 2931-2942, 2000.

[9] M. Brachet, M. Meneguzzi and S. Sulem, "The dynamics of freely decaying two-dimensional turbulence", J. Fluid Mech. 194, 333-349, 1988.

[10] H. Brands, J. Stulemeyer, R.A. Pasmanter and T.J. Schep, "A mean field prediction of the asymptotic state of decaying 2D turbulence" *Phys. Fluids* **9** (10), 2815, 1997; comments by W.J. Matthaeus and D. Montgomery and authors' answer, Phys. Fluids 10 (5), 1237-1238, 1998.

[11] H. Brands, P. H. Chavanis, R. Pasmanter and J. Sommeria "Maximum entropy versus minimum enstrophy vortices", Phys. Fluids 11 (11), 3465-3477, 1999.

[12] H.W. Capel and R.A. Pasmanter "Evolution of the vorticity-area density during the formation of coherent structures in two-dimensional flows" (e-print chao-dyn/9908010).

[13] G.F. Carnevale and G. K. Vallis "Pseudo-advective relaxation to stable states of inviscid two-dimensional fluids" J. Fluid Mech. 213, pp 549-571, 1990.

[14] G. F. Carnevale, J. C. Mc Williams, Y. Pomeau, J. B. Weiss and W. R. Young "Evolution of vortex statistics in two-dimensional turbulence", Phys. Rev. Lett. 66, 2735-2738, 1991.

[15] S.A. Chaplygin "One case of vortex motion in fluid" Proc. Phys. Sec. Natural Philos. Soc. 11, 114, 1902.

[16] J. R. Chasnov, On the decay of two-dimensional homogeneous turbulence, Phys. Fluids 9 (1), 1997.

[17] P. H. Chavanis, "Systematic drift experienced by a point vortex in two-dimensional turbulence", *Phys. Rev. E* 58, R1199-1202, 1998.

[18] P. H. Chavanis P.H "From Jupiter's great red spot to the structure of galaxies: statistical mechanics of two-dimensional vortices and stellar systems" in Nonlinear Dynamics and Chaos in Astrophysics: a Festschrift in Honor of George Contopoulos. Annals of the New York Academy of Sciences 867, 120-141, 1998.

[19] P. H. Chavanis "Quasilinear theory of the 2D Euler equation", Phys. Rev. Lett. 84, 5512-5515, 2000.

[20] P. H. Chavanis et C. Sire"The spatial correlations in the velocities arising from a random distribution of point vortices" (arXiv:cond-mat/0004410), to appear in Phys. Fluids.

[21] P. H. Chavanis and J. Sommeria, "Classification of self-organized vortices in two-dimensional turbulence : the case of a bounded domain" J. Fluid Mech. 314, 267-297, 1996.

[22] P.H. Chavanis and J. Sommeria, "A thermodynamic approach to small scale parameterization in 2D turbulence", Phys. Rev. Lett. 78, 3302-3305, 1997.

[23] P. H. Chavanis and J. Sommeria, "Classification of robust isolated vortices in two-dimensional hydrodynamics" J. Fluid Mech. 356, 259-296, 1998.

[24] P. H. Chavanis. and J. Sommeria."Statistical mechanics of the shallow water system" submitted to Phys. Fluids (e-print physics/0004056), 2001.

[25] P. H. Chavanis, J. Sommeria and R. Robert, "Statistical mechanics of two-dimensional vortices and collisionless stellar systems " Astrophys. J. 471, 385-399, 1996.

[26] A. J. Chorin, Vortex methods, in "Les Houches LVIX, Computational fluid dynamics" 65-109, North-Holland, 1993.

[27] A. J. Chorin, Vorticity and turbulence, Springer, 1994.

[28] G. H. Cottet Analyse numrique des mthodes particulaires pour certains problmes non-linaires. Thse Univ. Paris VI., 1987

[29] G.H. Cottet and Koumoutsakos "Vortex methods" Cambridge Univ. Press 2000.

[30] Y. Couder, "Two-dimensional grid turbulence in a thin liquid film", J. Phys. Lett. (Paris) 45, 353-360, 1984.

[31] Y. Couder and C. Basdevant, "Experimental and numerical study of vortex couples in two dimensional flows", J. Fluid Mech. 173, 225-251, 1986.

[32] P. Davidson, "The role of angular momentum in isotropic turbulence: Part 2, two-dimensional turbulence", submitted to J. Fluid Mech.

[33] M.A. Denoix., J. Sommeria and A. Thess "Two-dimensional turbulence: the prediction of coherent structures by statistical mechanics", in "Progress in Turbulence Research", Ed. Branover H. and Unger Y., A.I.A.A., pp 88-107, 1994.

[34] D.G. Dritschel, A general theory for two-dimensional vortex interactions, J. Fluid Mech. 293, 269-303, 1995.

[35] G. L. Eyink "Exact results on stationary turbulence in 2D: consequences of vorticity conservation", Physica D 91, 97-142, 1996.

[36] G. L . Eyink and H. Spohn, "Negative temperature states and large-scale long-lived vortices in two-dimensional turbulence", J. Stat. Phys. 70, 833-886, 1993.

[37] G. Falkovitch and V. Lebedev, "Universal direct cascade in two-dimensional turbulence", Phys. Rev. E 50 (5), 1994.

[38] G. Falkovitch, this book

[39] M. Farge, this book

[40] K. S. Fine, A. C. Cass, W. G. Flynn and C. F. Driscoll, "Relaxation of 2D turbulence to vortex crystal", Phys. Rev. Lett. 75, 3277-3280, 1995.

[41] U. Frisch "Turbulence: the legacy of A.N. Kolmogorov" Cambridge Univ. Press, 1995.

[42] U. Frisch and P.L. Sulem, "Numerical simulation of the inverse cascade in two-dimensional turbulence", Phys. Fluids 27, 1921-1923, 1984.

[43] S. Gama, M. Vergassola and U. Frisch, "Negative eddy viscosity in isotropically forced two-dimensional flow: linear and nonlinear dynamics", J. Fluid Mech. 260, 95-126, 1994.

[44] J. Goodman, T.Y. Hou and J. Lowengrub, "Convergence of the point vortex method for the 2D Euler equations", Comm. Pure and Appl. Math. XLIII, 415-430, 1990.

[45] A. Hasegawa, "Self-organization processes in continuous media" Advances in Physics 34 (1), 1-42, 1985.

[46] G.J.F. van Heijst and J.B. Flor, Dipole formation and collisions in a stratified fluid, Nature 340, 212-215, 1989.

[47] G.J.F van Heijst ., P. A. Davies and R. G. Davis "Spin-up in a rectangular container" Phys. Fluids A2, 150, 1990.

[48] G. J. F. van Heijst and Kloosterziel "Tripolar vortices in a rotating fluid" Letter to Nature 338, 569-571, 1989.

[49] J. Herring and J. McWilliams, "Comparison of direct numerical simulation of two-dimensional turbulence with two-point closure: the effect of intermittency" J. Fluid Mech. 153, 229-242, 1985.

[50] G. Holloway "Representing topographic stress for large-scale ocean models", J. Phys. Ocean. 22, 1033, 1992.

[51] D. Z. Jin and D. H. E. Dubin "Regional maximum entropy theory of vortex crystal formation", Phys. Rev. Lett. 80 (20), 4434-4437, 1998.

[52] G. Joyce and D. Montgomery "Negative temperature states for the two-dimensional guiding-centre plasma" J. Plasma Physics 10 (1), pp 107-121, 1973.

[53] B. Juttner., A. Thess and J. Sommeria, "On the symmetry of self-organized structures in two-dimensional turbulence", Phys. Fluids 7 (9), 2108-2110, 1995.

[54] T. Kato, "On the classical solutions of the two-dimensional non stationary Euler equation". Arch. Rat. Mech. Anal. 25, p.302-324, 1967.

[55] Yu. B. Kolesnikov and A. B. Tsinober, "An experimental study of two-dimensional turbulence behind an array" Isv. Akad. Nauk SSSR Mech. Zhid. i Gaza 4, 146, 1974.

[56] R. H. Kraichnan, "Inertial ranges in two-dimensional turbulence" Phys. Fluids 10, 1417-1423, 1967.

[57] R. H. Kraichnan, "Statistical dynamics of two-dimensional flow", J. Fluid Mech. 67, 155-175, 1975.

[58] R.H. Kraichnan and D. Montgomery, Two-dimensional turbulence, Rep. Prog. Phys. 43, pp 547-617, 1980.

[59] G.A. Kuz'min, "Statistical mechanics of the organization into two-dimensional coherent structures" in "Structural Turbulence", Acad. Naouk CCCP Novosibirsk, Institute of Thermophysics, Ed. Goldshtik M.A., pp 103-114, 1982.

[60] Lamb H., Hydrodynamics, Dover, 1932.

[61] J. P. Laval, B. Dubrulle and S. Nazarenko, "Nonlocality of interaction of scales in the dynamics of 2D incompressible fluids", submitted Phys. Fluids.

[62] C.E. Leith, "Minimum enstrophy vortices". Phys. Fluids, 27, 1388-95, 1984.

[63] B. Legras, P. Santangelo and R. Benzi, "High resolution numerical experiments for forced two-dimensional turbulence", Europhys. Lett. 5, 37-42, 1988.

[64] M. Lesieur, "Turbulence in fluids", Kluwer Academic, 1990.

[65] M. Lesieur, C. Staquet, P. Le Roy and P. Comte, "The mixing layer and its coherence examined from the point of view of two-dimensional turbulence", J. Fluid Mech. 192, 511-534, 1988.

[66] E. Lindborg, "Can the atmospheric kinetic energy spectrum be explained by two-dimensional turbulence?", J. Fluid Mech. 388, 259-288, 1999.

[67] E. Lindborg and K. Alvelius "The kinetic energy spectrum of the two-dimensional enstrophy turbulence cascade", Phys. Fluids 12 (5), 2000.

[68] D. Lynden-Bell, "Statistical Mechanics of Violent Relaxation in Stellar Systems, "Monthly Notes of the Royal Astronomical Society, Vol.136, 1967, pp.101-121.

[69] P. S. Marcus, "Vortex dynamics in a shearing zonal flow", 215, 393 - 430, 1990.

[70] D. Marteau D., O. Cardoso and P. Tabeling, "Equilibrium states of 2D turbulence: an experimental study", Phys. Rev. E 51, 5124, 1995.

[71] B.K. Martin, X.L. Wu, W.I. Goldburg and M.A. Rutgers, "Spectra of decaying turbulence in a soap film", Phys. Rev. Lett. 80, 3964, 1998.

[72] Meleshko V.V. and van Heijst G.J.F., On Chaplygin's investigations of 2D vortex structures in an inviscid fluid, J. Fluid Mech. 272, 157-182, 1994.

[73] J. Michel and R. Robert, "Statistical mechanical theory of the Great Red Spot of Jupiter"J. Stat. Phys. 77, (3/4) 645-666.

[74] J. Miller "Statistical mechanics of Euler equations in two dimensions", Phys. Rev. Lett. 65, 17, 2137-2140, 1990.

[75] T.B. Mitchell and C. F. Dritscoll "Electron vortex orbits and merger" Phys. Fluids 8 (7), 1828-1841, 1996.

[76] J.M. Nguyen Duc , P. Capran & J. Sommeria "Experimental investigation of the two-dimensional inverse energy cascade", dans "Current Trends in Turbulence Research", vol.112 of Progress in Astronautics and Aeronautics, A.I.A.A, p 78-86, 1988.

[77] J. M. Nguyen Duc, J. Sommeria, Experimental characterization of steady two-dimensional vortex couples. J. Fluid Mech.,192, p. 175-192, 1988.

[78] E. A. Novikov "Dynamics and statistics of a system of vortices". Sov. Phys. JETP. 41, p. 937-43, 1976.

[79] L. Onsager, "Statistical hydrodynamics" Nuovo Cimento Suppl. 6, 279-287, 1949.

[80] S. Ossia, "Simulation numrique des chelles infrarouges en turbulence isotrope incompressible", Thse INPG-Grenoble, France, 2000.

[81] E. A. Overman, N.J. Zabusky, "Evolution and merging of isolated vortex structures". Phys. Fluids 25, p. 1297, 1982.

[82] Paret J., Jullien M.C. and Tabeling P., Vorticity statistics in the two-dimensional enstrophy cascade, Phys. Rev. Lett. 83 (17) , 3418-3421, 1999.

[83] Paret J. and Tabeling P., Intermittency in the two-dimensional inverse cascade of energy: experimental observations, Phys. Fluids 10 (12), 3126-3136, 1998.

[84] Y.B. Pointin and T. S. Lundgren "Statistical mechanics of two-dimensional vortices in a bounded container", Phys. Fluids 19 (10), 1459-1470, 1976.

[85] R. Robert, "Etat d'\'equilibre statistique pour l'\'ecoulement bidimensionnel d'un fluide parfait", C.R. Acad. Sci. Paris t 311, S\'erie I, 575-578, 1990.

[86] Robert R. & Rosier C. "The modelling of small scales in 2D turbulent flows: a statistical mechanics approach" J. Stat. Phys. 86, 481, 1997.

[87] R. Robert and C. Rosier, "Long range predictability of atmospheric flows", Nonlinear Proc. Geophysics, in press.

[88] R. Robert and J. Sommeria"Statistical equilibrium states for two-dimensional flows", J. Fluid Mech. 229, 291-310, 1991.

[89] R. Robert and J. Sommeria, "Relaxation towards a statistical equilibrium state in two-dimensional perfect fluid dynamics" Phys. Rev. Letters 69 , 2776-2779, 1992.

[90] R. Robert, "On the Statistical Mechanics of 2D Euler Equation", Comm. Math. Phys. 212 (1), 245-256, 2000.

[91] P. G. Saffman, "Vortex Dynamics", Cambridge University Press, 1995.

[92] D. Serre, "Les invariants du premier ordre de l'quation d'Euler en dimension trois". Physica 13D, p.105-136, 1984.

[93] C. E. Seyler, Y. Salu, D. Montgomery and G. Knorr, Phys. Fluids 18, 803-813, 1975.

[94] C. Sire and P. H. Chavanis "Numerical renormalization group of vortex aggregation in 2D decaying turbulence: the role of three-body interactions", submitted to Phys. Rev. E, 6644-6653, 2000.

[95] R. A. Smith and T. M. O'Neil, "Non-axisymmetric thermal equilibria of a cylindrically bounded guiding center plasma of discrete vortex system", Phys. Fluids B 2 (12), 2961-2975.

[96] L. M. Smith and V. Yakhot, "Finite size effects in forced two-dimensional turbulence", J. Fluid Mech. 274, 115, 1994.

[97] J. Sommeria, 1986 "Experimental study of the two-dimensional inverse energy cascade in a square box" J. Fluid Mech. 170, pp139-168.

[98] J. Sommeria, C. Staquet and R. Robert, "Final equilibrium state of a two-dimensional shear layer", J. Fluid Mech. 233, 661-689, 1991.

[99] J. Sommeria "Statistical mechanics of potential vorticity for parameterizing mesoscale eddies, in Ocean modeling and parameterization, Ed. Chassignet P. and Verron J., NATO Science Series C, 516, 303-326, 1998.

[100] J. Sommeria, S.D. Meyers, H.L. Swinney, "Laboratory simulation of Jupiter's Great Red Spot". Nature, 331, 1, 1988.

[101] S. Sukoriansky, B. Galperin and A. Chekhlov, "Large scale drag representation in simulations of two-dimensional turbulence", Phys. Fluids 11, 3043-3053, 1999.

[102] P. Tabeling, S. Burkhart, O. Cardoso and H. Willaime "Experimental study of freely decaying two-dimensional turbulence" Phys. Rev. Lett. 67, 3772, 1991.

[103] H. Tennekes and J.L. Lumley, "A first course in turbulence", MIT Press, 1974.

[104] A. Thess & J. Sommeria "Two-dimensional turbulence: transition", in "Progress in Turbulence Research", Ed. Branover H. & Unger Y., A.I.A.A., 80-87, 1994.

[105] B. Turkington, "Statistical equilibrium measures and coherent states in 2D turbulence" Comm. Pure and App. Math. 52, 781, 1999.

[106] B. Turkington, B. and N. Whitaker, "Statistical equilibrium computations of coherent structures in turbulent shear layers", SIAM J. Sci. Comput. 17 (16), 1414, 1996.

[107] J. Mc Williams, "The emergence of isolated coherent vortices in turbulent flow", J. Fluid Mech. 146, 21-43, 1984.

[108] V. I. Youdovitch, "Non stationary flow of an ideal incompressible liquid". Zh. Vych. Mat. 3, p. 1032-66, 1963.